UNIVERSIDADE DE LISBOA
FACULDADE DE CIÊNCIAS
DEPARTAMENTO DE ENGENHARIA GEOGRÁFICA, GEOFÍSICA E ENERGIA

Technical evaluation and modelling of a cross wind kite based on Loyd's model

Nuno Miguel França Sena Lourenço

Mestrado Integrado em Engenharia da Energia e do Ambiente

Dissertação orientada por:
Engenheiro Tiago Mendes Duarte
Professor Fernando Marques da Silva

2018

Agradecimentos

A realização desta dissertação de mestrado contou com o apoio e incentivo de pessoas às quais estarei eternamente grato.

Ao meu orientador Engenheiro Tiago Mendes Duarte, pela disponibilidade em receber-me semanalmente, partilha de conhecimentos, expor opiniões e críticas de forma construtiva, colaboração na procura de soluções, quando surgiam problemas e dúvidas ao longo da realização deste trabalho.

Ao professor Fernando Marques da Silva, pela sua disponibilidade em aceitar ser meu co-orientador, pela clareza, rigor, apoio teórico na área de aerodinâmica e manifestação das suas opiniões e críticas.

À minha namorada Sara Marcelo e ao meu amigo Telmo Batalha, que estiveram sempre ao meu lado durante esta fase, pelo companheirismo, força e apoio em certos momentos difíceis.

Por fim, tendo consciência que sozinho nada disto teria sido possível, dirijo um agradecimento especial aos meus pais, pela educação e valores que me transmitiram, por me darem a oportunidade de estudar, por serem modelos de coragem, apoio e incentivo e definirem muito da pessoa que sou hoje. A eles dedico este trabalho!

Resumo

Ao longo do seu desenvolvimento, o ser humano sempre necessitou de recorrer a fontes de energia para satisfazer as suas necessidades básicas, quer na forma de calor ou trabalho. As fontes de energia renováveis que tal como o nome indica, são fontes inesgotáveis e sem qualquer tipo de emissões poluentes para o ambiente, surgiram como uma alternativa às fontes de energia de origem fóssil (petróleo, gás natural e carvão) e nuclear. Alguns exemplos destas fontes de energia renovável são: vento, sol, biomassa, ondas e marés, hídrica e geotermia.

A energia que potencialmente pode ser gerada pelo vento seria suficiente para suprir toda a procura energética no mundo (entre 81-118 PWh/ano). No entanto, este potencial nem sempre é aproveitado devido a certas restrições, como a localização do parque eólico ou a limitação da altura das turbinas. As tecnologias para geração de energia eólica a altas altitudes, com cotas superiores a 100 metros, pretendem minimizar parte desses problemas, uma vez que a estas alturas o vento sopra com maior velocidade. A principal preocupação é entender se estas tecnologias também podem competir com as turbinas eólicas convencionais em termos de produção de energia, com melhor relação qualidade-custo. Este tipo de tecnologia tem o potencial de reduzir o custo de investimento, porque tem uma estrutura menos complexa do que uma turbina convencional e aumenta a energia produzida, acedendo a lugares de maior potencial eólico, o que resulta num menor custo unitário de energia. No entanto, é preciso ter em conta que o preço por kilograma do material tipicamente utilizado nestas tecnologias, a fibra de carbono, é bastante superior ao preço do aço utilizado na construção das estruturas das turbinas eólicas. No protótipo criado pela Makani, alega-se um custo unitário de energia de 0.026 €/kWh, um valor consideravelmente menor quando comparado com o de uma turbina convencional de 2.5 MW que ronda os 0.078 €/kWh.

A principal objetivo desta dissertação é avaliar o potencial energético que é possível atingir com o protótipo “M600”, desenhado pela Makani. Esta tecnologia tem como base um planador com 26 metros de envergadura com oito pequenos rotores dispostos ao longo das suas asas. Estes rotores ao serem atravessados pelo vento, produzem energia sendo esta transmitida para uma estação no solo através de um cabo condutor elétrico com cerca de 400 metros. A fibra de carbono que constitui o corpo do planador concede lhe uma alta resistência à tração, e um baixo peso que favorece as suas manobras durante o voo. O cabo condutor elétrico, revestido também por fibra de carbono, apresenta no seu interior alumínio, um material com uma baixa impedância elétrica, sendo por isso um bom condutor elétrico, garantindo que as perdas de energia na sua transmissão são mínimas. O planador arranca do seu ponto inicial, com o plano das asas em posição vertical e com os rotores a trabalharem como propulsores para fazê-lo levantar voo, consumindo energia elétrica. O sistema ascende, e quando o cabo está completamente estendido, este entra no modo de voo livre, descrevendo uma trajetória circular restringida pelo comprimento do cabo. Neste modo de voo, os rotores funcionam como geradores que convertem o poder do vento em energia elétrica. Quando o vento não é suficiente para o dispositivo se manter no ar, ou por qualquer outro motivo este tem de aterrar, o sistema muda novamente o seu modo de voo, para poder aterrar no solo. Durante as fases de arranque e aterragem do sistema, a energia consumida é uma pequena fração da energia que é produzida no modo de voo livre.

Para simular a operação e o comportamento deste equipamento, foi implementado um modelo numérico, proposto por Miles L. Loyd no seu artigo de 1980 "Crosswind Kite Power", com o auxílio do programa informático *Simulink*. No modelo proposto por Loyd, os seus cálculos foram realizados tendo como base um avião militar com 68 metros de envergadura e cerca de 230 toneladas. Numa primeira aproximação,

a simulação em *Simulink* foi testada nas mesmas condições que as do modelo criado por Loyd, até os resultados da simulação se aproximarem dos obtidos por ele mesmo. Após isto acontecer, o modelo foi testado tendo com os valores do protótipo da Makani, o "M600", para se poder estudar o seu comportamento. Com esta simulação foi possível concluir que o "M600" descreve um trajeto circular com um tamanho da órbita de 0.4 radianos, a uma velocidade de aproximadamente 98.7 m/s, variando entre altitudes de 75 até 363 metros. Foi criado também um modelo do vento baseado numa Lei de Potência com a velocidade deste a oscilar entre 8.66 e 10.86 m/s. Esta simulação permitiu ainda concluir que este protótipo teria uma potência média à saída de 0.598 MW aquando da realização de três ciclos completos de rotação, valor bastante próximo da potência nominal do "M600": 0.6 MW. Verificou-se ainda que em alguns momentos a potência registada à saída excedia a potência nominal, pelo que os geradores poderão ter de ser sobredimensionados para aceitar estes valores, uma vez que de outra forma estariam a desperdiçar energia. Alternativamente, este fenómeno pode ser controlado com arrasto adicional provocado por *flaps* nas asas ou pelos próprios rotores, que levam a uma redução da potência média por ciclo. Este processo deve ser assegurado por controladores abordo do sistema. A tensão máxima criada no cabo pelo planador foi de aproximadamente 486 kN, sendo este capaz de suportar estas tensões.

Na realização desta dissertação não foi possível prever de forma concreta o comportamento do controlador do movimento do planador recorrendo a um PID (controlador Proporcional Integral Derivativo). Apesar desta hipótese ter sido testada, os seus resultados foram inconclusivos, com o planador a descrever uma trajetória bastante irregular, inclusivamente atravessando o solo com o registo de cotas negativas. Tendo por base o artigo de Loyd, este controlador é definido como a tangente do ângulo de rolamento, que representa a rotação realizada em torno do eixo longitudinal do planador. Para esse fim, foi feita uma aproximação deste ângulo forçando o planador a descrever um movimento circular uniforme a uma velocidade constante, variando este ângulo entre -7 e 47 graus nos pontos de maior e menor cota respetivamente. Nos pontos médios da ascensão e descida, à mesma cota, quando este está perfeitamente perpendicular à direção vento, o ângulo de rolamento foi considerado zero. Após vários testes, a velocidade constante de rotação para o qual os resultados obtidos mais se aproximavam aos obtidos por Loyd, foi a de 5.5 RPM, com menores erros relativos registados. O facto de o planador descrever uma velocidade constante pode trazer algumas incertezas ao modelo, impossibilitando o cálculo de algumas características desta tecnologia como a curva de potência ou o fator de capacidade. No entanto fica em aberto um futuro estudo para poder prever o comportamento de um controlador mais elaborado num eixo com seis graus de liberdade.

Palavras chave: "M600" Makani, Miles Loyd, energia eólica de alta altitude, Simulink, energia renovável

Abstract

The potential energy that can be generated by wind should be sufficient to supply all the energy demand in the world (between 81-118 PWh /year). However, this potential is not always harnessed due to certain constraints such as the location of the wind farm and the limitation of turbine heights.

The technologies for wind power generation at high altitudes, with heights higher than 100 meters, intend to settle some these problems. The main concern is to understand if these technologies can also compete with the conventional wind turbines in terms of energy production, with better cost-quality relation. This type of technology has the potential to reduce the investment cost, due to a less complex structure than a conventional turbine, and increase the energy produced accessing to higher wind potential places, resulting in a lower levelized cost of energy. For Makani's prototype, a levelized cost of energy of 0.026 € / kWh is claimed, a considerably lower value when compared to a conventional 2.5 MW turbine that is around 0.078 € / kWh.

The main objective for the development of this dissertation is to evaluate the energy potential that can be achieved with the "M600" Makani prototype. This technology is based on a crosswind kite that produces energy through mini rotors placed on-board the kite. This energy is transmitted to a ground station through an electric conductor tether. To simulate the operation and the behaviour of this equipment was implemented with the help of *Simulink* software, the numerical model proposed by Miles L. Loyd in his article "Crosswind Kite Power".

After this simulation was possible to conclude that this prototype describes a circular path with an orbit size of 0.4 radians, at a velocity of approximately 98.7 m/s, varying between altitudes of 75 and 363 meters. A wind model was also created based on a Power Law, with the wind oscillating between 8.66 and 10.86 m / s. This simulation also led to the conclusion that this prototype would have an average power output of 0.598 MW after three complete cycles of rotation were performed, a value similar to the 0.6 MW of nominal power of the "M600". The peak tether tension was approximately 486 kN, being able to withstand the proposed stresses.

In this dissertation realization wasn't possible to predict concretely the controller behaviour of the kite movement using a PID, since the results were inconclusive. Based on Loyd's article, this controller was defined as the role angle's tangent, so an approximation of this angle was made forcing the kite to describe the desired motion at a constant speed of 5.5 RPM per cycle. This factor can bring some uncertainties to the model and makes it impossible to calculate some characteristics of this technology as the power curve or the capacity factor, however a future study is still open to be able to predict this controller behaviour.

Keywords: "M600" Makani, Miles Loyd, cross wind kite, high altitude wind power, renewable energy, Simulink

Contents

List of Figures

List of Tables

Acronyms and Abbreviations

ABL	Atmospheric Boundary Layer
AEP_t	Annual Energy Production (at the year t)
AIAA	American Institute of Aeronautics and Astronautics
AWES	Airborne Wind Energy Systems
CapEx	Capital Expenditures
FAA	Federal Aviation Administration
FEG	Flying Electric Generator
FG-AWES	Fly-Generator Airborne Wind Energy Systems
GG-AWES	Ground-Generator Airborne Wind Energy Systems
LCOE	Levelized Cost of Energy
LEI	Leading Edge Inflatable
LEMAP	Long Endurance Medium Altitude Platform
MBD	Model-Based Design
NTS	Nature Technology Systems
$OpEx_t$	Operational Expenditures (at the year t)
PID	Proportional–integral–derivative controller

RPM	Rotations Per Minute
SI	International System of Units (SI, abbreviated from the French "*Système international*")

Notations

a	Acceleration [m/s^2]
A	cross-sectional area intersected by the wind [m^2]
A_k	Wings reference area of kite [m^2]
C	Tangent of roll angle
C_D	Kite coefficient of drag
C_{DT}	Tether coefficient of drag
C_L	Kite coefficient of lift
d	Tether cross-sectional diameter [m]
D	Total drag [N]
D_k	Kite drag [N]
D_P	Power production drag [N]
D_T	Tether drag [N]
F	Force applied over an object in equation 2.21 [N]
F_C	Crosswind kite relative lift power [W]
F_D	Crosswind kite relative drag power [W]
F_s	Simple kite relative lift power [W]
g	Acceleration of gravity [m/s^2]
h	Altitude [m]
h_0	Surface roughness length [m]
h_{ref}	Reference quota [m]
H	Factor defined by equation 2.10

k	Von Kármán constant
$\vec{l}$	Unit vector in θ direction
L	Kite lift [N]
$\vec{m}$	Unit vector in ∅ direction
$\vec{n}$	Unit vector in radial direction
P	Power produced (W)
P_{inc}	Incident wind power (W)
r	Distance travelled in equation 2.21 [m]
R	Spherical coordinate and tether length [m]
t	Elapsed time (s)
T	Tether tension at kite [N]
u	Unit vector representative of orbit axis of rotation in Rodrigues formula
u_*	Friction velocity in the ground [m/s]
U	Wind velocity in the characterization of wind model [m/s]
U_{ref}	Reference velocity of wind [m/s]
v	Vector defined in R^3 in Rodrigues formula
v_{rot}	Rotation vector defined in R^3 in Rodrigues formula
V	Kite velocity [m/s]
V_A	Relative velocity through air [m/s]
V_C	Crosswind velocity of a kite in lift power production [m/s]
V_L	Load velocity of a kite in lift power production [m/s]
V_l	Velocity component in θ direction [m/s]

V_m	Velocity component in ∅ direction [m/s]
V_n	Velocity component in radial (R) direction [m/s]
V_w	Wind velocity [m/s]
w	Work [J]
W	Kite weight [N]
W_T	Tether weight [N]
x,y,z	Cartesian coordinates
α	Wind model parameter defined in equation 3.4
β	Position defined by the time function of the angular position of a uniform circular motion [rad]
β_0	Initial position defined by the time function of the angular position of a uniform circular motion [rad]
$\dot{\beta}_0$	Derivative of β_0 that represents the velocity of rotation in the time function of the angular position of a uniform circular motion [rad/s]
$\theta, \emptyset$	Spherical coordinates [rad]
$\dot{\theta}, \dot{\emptyset}$	First derivative of θ and ∅ respectively and angular velocity components [rad/s]
$\ddot{\theta}, \ddot{\emptyset}$	Second derivative of θ and ∅ respectively and angular acceleration components [rad/s^2]
ρ	Air density [kg/m^3]
ρ_T	Tether density [kg/m^3]
σ	Tether working stress [Pa]
φ	Angle of rotation in Rodrigues formula [rad]

Chapter 1. Introduction

1.1 General Framework

Energy resources have been used by mankind for thousands of years to satisfy some of their basic needs in the form of heat and work, and their availability is one of the main factors for the development of humanity.

The growth in world's population led, in the last century, to an exponential increase of the demand and use of electricity and fossil fuels, including coal, petroleum and natural gas. Despite the benefits that fossil fuels have brought us in the last century, serious concerns make them unfeasible for the development of society due to their finiteness and pollution they cause to the environment. Therefore, it's essential to generate alternative sources called renewable energies, that can satisfy the ever-growing energy necessities of human beings without compromising their environment.

Many alternatives to fossil fuels are available and the investment in this area doubled, in developed countries, between 1990 and 2000 [1]. Some examples of renewable energies are: wind, solar, geothermal, hydropower, tidal and biomass energies. The current state of growth and development of our society requires a growing, and often unsustainable exploitation of natural resources, which allows the creation and scenario predictions in which renewable energy will be the only solution for a society that is increasingly in need of new forms of energy.

Traditionally, wind turbines are used to harness wind energy, which require no fuel and do not produce toxic neither radioactive wastes. Still, they are huge fixed constructions, and, although they undergo a lot of research and development to improve their efficiency, they will have reached their limits. According to a 2005 study of the Standford University [2], the potential that can be generated by wind is sufficient to supply all the energy demand in the world (between 81-118 PWh/year). However, this potential is not always harnessed due to certain constraints such as the location of the wind farm and the limitation of turbine heights. At present, the highest wind turbine reaches 200 meters, where the wind is still unstable but with an acceptable speed in order to produce energy [3]. The atmospheric boundary layer is the part of the troposphere that is directly influenced by the presence of the Earth's surface, which depending on its roughness has a determinant influence in the wind speed behaviour, which usually increases with altitude [4]. It is known that the power generated by wind turbines increases with the cube of wind velocity (equation 1.1), and higher velocities are expected for higher altitudes (Figure 1.1). In fact, strong wind could be present at higher altitudes with little or no wind at low altitudes.

$$P_{inc} = {}^{1}/_{2}\,\rho A V_w{}^{3} \tag{1.1}$$

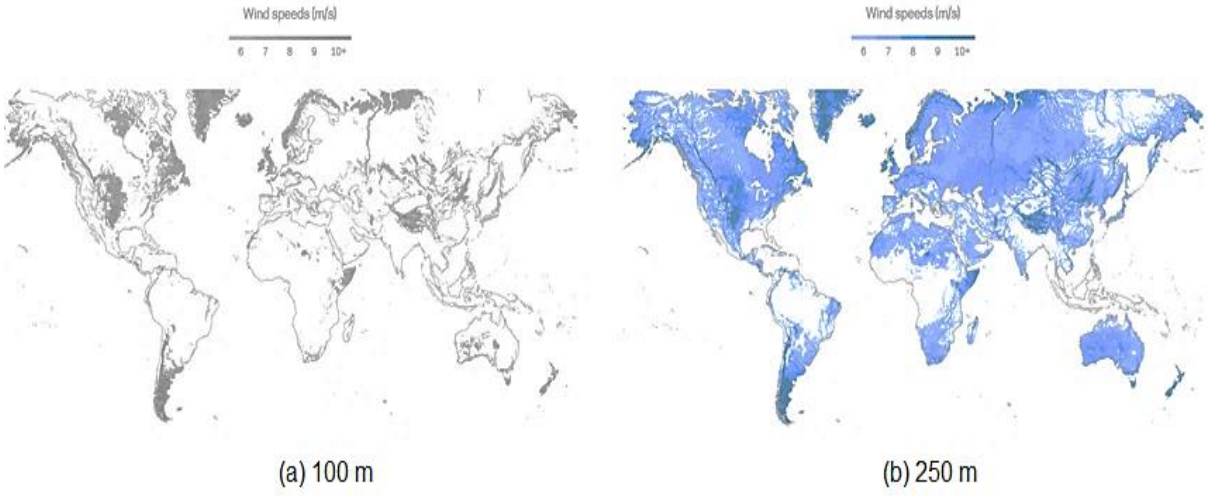

Figure 1.1 Map of average wind speed (m / s) with height of 100m (a) and 250m (b) above surface level [5]

To overcome this typical wind-turbine limitation, new solutions to extract energy from high altitudes winds are still being investigated [3]. The main concern of these technologies is to understand if they can also compete with the conventional wind turbines in terms of energy production and with a lower levelized cost of energy (LCOE). This parameter is obtained by the following formula:

$$LCOE(€/MWh) = \frac{CapEx + \sum_{t=1}^{n} \frac{OpEx_t}{(1+i)^t}}{\sum_{t=1}^{n} \frac{AEP_t}{(1+i)^t}} \quad (1.2)$$

The numerator of the latter represents the sum of the capital (initial investment) plus the operational and maintenance expenditures throughout its lifetime, and the denominator represents the amount of energy production over its lifetime too, updated with the discount rate (i). The goal of these new technologies for wind extraction at higher altitudes is to increase the denominator and reduce the numerator to decrease the LCOE.

1.2 State of the Art

In 1980, an American electrical engineer, member of AIAA, called Miles L. Loyd suggested that lifting a wind turbine into the atmosphere, at some significant distance above the ground, where winds tend to blow more consistently and at greater speed than they do at ground level, could increase the energy production significantly. Loyd thought that if a kite's aerodynamic surface converts wind energy into motion of the kite, this motion could be converted into useful power by driving turbines on the kite or by pulling a load on the ground. His propositions where published in a paper called "Crosswind Kite Power (for Large-Scale Wind Power Production)" in the Journal of Energy [6], where he predicted that such turbines could generate electricity at a significant greater magnitude and more consistently than they could if build on the ground.

Loyd's suggestion was largely ignored for many years but has received considerably more attention in the second decade of the twenty-first century. Many companies are still working on designing and/or constructing of one or more variations of Loyd's so-called airborne wind turbine, also known as Airborne Wind Energy Systems (AWES) [7]. So far, many prototypes were tested whit the production of energy, however they weren't tested long enough to be marketed.

These systems have two ways to operate [8][9]:

- In Ground-Generator Airborne Wind Energy Systems (GG-AWES), electrical energy is produced on the ground by mechanical work done by traction force, transmitted from the aircraft to the ground system through one or more ropes, which produce the motion of an electrical generator. Among GG-AWES we can distinguish between fixed-ground-station devices, where the ground station is fixed to the ground and moving-ground-station systems, where the ground station is a moving vehicle (Figure 1.2a).

- In Fly-Generator Airborne Wind Energy Systems (FG-AWES), electrical energy is produced on the aircraft and it is transmitted to the ground through a special rope which carries electrical cables. In this case, electrical energy conversion is generally achieved using wind turbines. FG-AWES produces electric power continuously while in operation, except during take-off and landing manoeuvres in which energy is consumed. Among FG-AWES it is possible to find crosswind systems and non-crosswind systems depending on how they generate energy (Figure 1.2b).

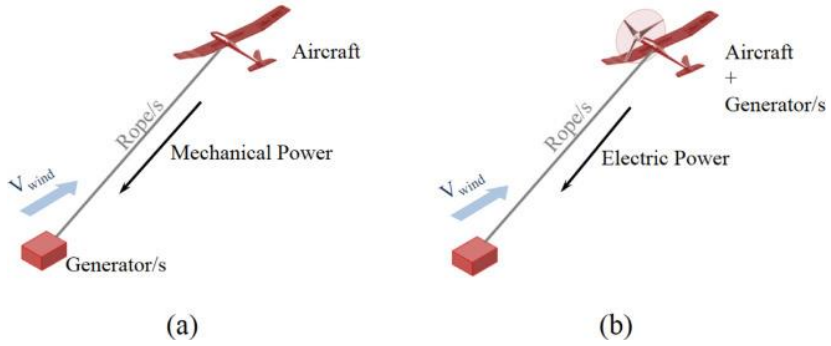

Figure 1.2 Airborne Wind Energy Systems. Ground Generation (a) and Fly Generation (b) [8]

1.2.1 Ground-Gen Airborne Wind Energy Systems

As previously anticipated, this kind of devices can be distinguished with fixed or moving ground stations.

The fixed ground station GG-AWES (or Pumping Kite Generators) are among the most exhaustively studied by private companies and academic research laboratories. Energy conversion is achieved with a two-phase cycle composed by a generation phase, in which electrical energy is produced, and a recovery phase, in which energy is consumed. In the generation phase (Figure 1.3a) the aircraft is driven in a way to produce a lift force and consequently a traction force (unwinding) on the ropes that induce the rotation

of the electrical generators producing energy. In the recovery phase (Figure 1.3b) motors rewind the ropes bringing the aircraft back to its original position from the ground. To have a positive balance, the net energy produced in the generation phase must be larger than the energy spent in the recovery phase.

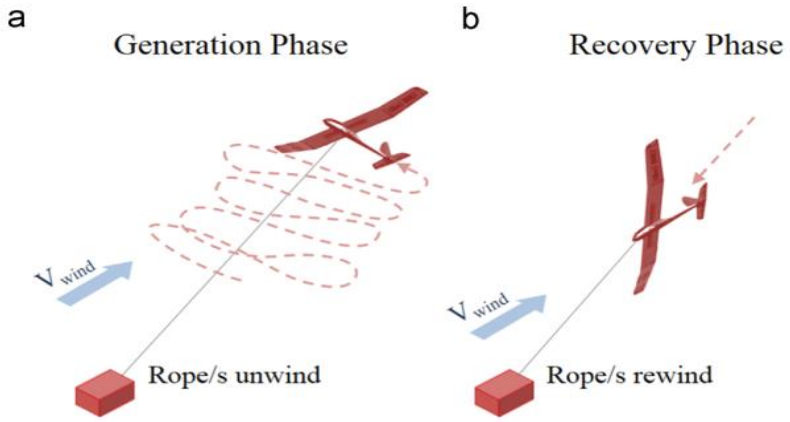

Figure 1.3 Scheme of the two-phase discontinuous energy production for GG-AWES: Generation (a) and recovery (b) phases [8]

The Italian KiteGen Research was one of the first companies to test a prototype of GG-AWES. The technology developed by this company called "*KiteGen Stem"* that could reach a nominal power of 3 MW, is based on an arch-kite that is controlled by two power-ropes winded on winches, that are driven by a pulley system through a 20 meters flexible rod, called 'stem', which is linked to the top of the ground station. At the beginning of the take-off manoeuvres, the kite is hanged upside down at the end of the stem, and once it takes off, the generation phase starts, in which the kite makes a crosswind flight with 'eight shaped' paths. At the same time ropes are unwinding causing the winches to rotate and the motor-generators transform mechanical power into electric power [10].

The Ampyx Power, a Dutch company, has developed a glider model that describes an 'eight shaped' path. After many prototypes, they are currently developing and testing the model AP3 that will be available in 2020. This device will have a wingspan of 12 meters, a power output of 250 kW and will achieve altitudes between 100 and 465 meters. This aircraft has a carbon fibre body, with on-board sensors and actuators (a rudder, an elevator and four flaperons- two ailerons and two flaps) to control the flight path. One tether connects the kite to a single winch in the ground station. When the device ascends, the tether is unwound due to the lifting force acting on the kite. Once the cable is fully extended (~ 900m), the kite descends from altitude, causing the tether to reel in. This cycle is repeated to the point where there is not enough wind to hold the device, so it lands autonomously in his platform, in the recovery phase [11].

Omnidea, a Portuguese company, designed a tethered inflatable and easily deployable platform. This one keeps the payload airborne by having her mildly lighter than air with the ability to generate by Magnus effect an aerodynamic lift force that withstands the drag imposed by wind. Since it is a tethered platform its subsystems can be permanently fed from the ground minimizing the need to land. This device called LEMAP is in its testing phase, so its power production is unknown [12].

At Delft University of Technology, research in kite power generation has been initiated by Professor Wubbo Ockels in 1993. The research group was established in 2005 and currently comprises 2 staff members, 5 researchers, and several MSc students. Recently, Delft University of Technology and

Karlsruhe University of Applied Sciences started a joint project to continue the development and testing of a tethered 20 kW experimental pumping kite generator. A main objective of this project is to improve the reliability and robustness of the technology and to demonstrate a continuous operation of 24 hours [13]. They demonstrated fully automatic operation of their 20 kW system in 2012 [14], with a LEI kite wing of 25m^2 wing surface. This prototype is based on a single tether and an airborne control pod, but they also control the angle of attack for powering and depowering the wing during production and recovery phase, respectively. An automatic launch and retrieval system for 100 m^2 LEI kites is under development for commercial application [13].

The Belgian university KU Leuven began its research on airborne wind energy systems in 2006. After significant theoretical contributions, the team developed a test bench to launch and landing a tethered glider with a pulley technique. This kite is brought up to speed by an arm rotating around a central axis. Once the airplane has gained enough speed, the tether can be unrolled, allowing the airplane to gain altitude [15]. They are currently developing a larger experimental test set-up, 2 m long with a 10 kW winch.

In addition to pumping systems, a few AWES concepts with moving-ground-station have been proposed. These ones are generally more complex systems, in which the aim is to provide an always positive power flow that makes it possible to simplify their connection to the grid by producing a continuously or nearly continuously energy. Differently from the pumping generator, the rope winding and unwinding is not producing/consuming significant power but is eventually used only to control the aircraft trajectory. The generation takes place thanks to the traction force of ropes that induces the rotation (or linear motion) of a generator that exploits the ground station movement rather than the rope winding mechanism. There are different concepts of moving-ground-station GG-AWES but only a few companies are working on systems like these and there are more patents and studies than prototypes under development.

The first moving-ground-station project has been proposed by Sequoia Automation and acquired by KiteGen Research. In this AWES concept called KiteGen Carousel, tethered aircrafts are fixed on the periphery of the rotor of a large electric generator with vertical axis. The aircraft forces make their ground stations rotate together with the rotor, which in turn transmits torque to the generator that convert it into electricity [16]. There is no prototype under development, but the concept has been simulated showing that 100 kites with 500 m^2 area could generate 1000 MW of average power with a wind speed of 12 m/s [17].

An alternative system based on ground stations that moves on closed track circuits has proposed by German company NTS [18]. Since 2011, NTS started testing a prototype where four tethered kites are controlled by a vehicle which moves on a 400 m flat straight railway track. They can produce up to 1 kW per m^2 of wing area with kites up to 40 m^2 [19]. The final product should have a closed loop railway where more vehicles run independently.

1.2.2 Fly-Generator Airborne Wind Energy Systems

As it was said before, in the FG-AWES the conversion of mechanical energy in electrical energy is done on the aircraft, being this energy transmitted to the ground by a tether that has both to conduct electricity and withstand a strong tension. These systems can be distinguished by its motion into crosswind or non-crosswind (stationary) systems.

The Californian company Sky Windpower [20] proposed a tethered rotorcraft called Flying Electric Generator (FEG) where conventional rotors generate power and simultaneously produce sufficient lift to keep the system aloft. Four rotors are arranged on an airframe, tethered to the ground by insulated aluminium conductors with Kevlar-type cords wrapping them. The aircraft can be supplied with energy, to be extended to a desired altitude and to reel the tether to retrieve the craft. When operating as a power source, two, four, or more rotors are inclined at an adjustable angle to the oncoming wind, generally up to 50º. The wind on the inclined rotors generates lift and forces rotation, which generates electricity [21]. Multiple rotors can be combined in a large-scale array to obtain more energy closer to jet streams. Jet streams are strong air currents, generated by the combination of the planet's rotation over its axis and atmospheric heating. Usually these are located near the boundaries of adjacent air masses with significant temperature differences, such as the transition from the troposphere (where temperature decreases with altitude) to the stratosphere (where the temperature increases with altitude) [22]. Sky Windpower tested two FEG prototypes. At 15 000 ft (4600 m) and above is possible to obtain individual rated outputs of up to 40 MW [21]. Unfortunately, the company went recently out of business.

The Altaeros Energies, company founded in 2010 at the Massachusetts Institute of Technology (MIT), conceived another stationary device: a tethered aerostat (industrial version of blimps and dirigibles) called Bat. The Bat is placed at 600 meters of altitude from the ground, tied to four conductor's cables, with a structure that contains helium, lighter than the air that simplifies the take-off and landing manoeuvres, and a rotor with three blades. The Bat concept is not much different from a normal wind turbine, with the difference of taking advantage of higher wind speeds at higher altitudes. This prototype has already been tested and is expected to produce twice the energy of a wind turbine at a conventional level [23].

Founded in 2008, the US company Joby Energy [24] developed a crosswind multi-frame structure with embedded aerofoils and turbines installed in his joints. Like other technologies, the take-off and landing manoeuvres are accomplished with energy consumption with the rotors of the turbines working as engines to move the device. Once the tether is fully unwound, the device takes a circular flight path powered by the wind and the rotors work as generators of energy [25] They claim that with a device with an output potential of 2 MW, operating at 2,000 feet of altitude (≈ 600 meters) can produce 2 GWh/year with a mean wind speed of 20 m/s.

The company Makani Power, developed also his own prototype, based on Loyd's work. This company was founded in 2006 with the goal of developing a low-cost renewable energy solution using kite technology [26]. In eight years, they developed and tested several AWES concepts including GG-AWES with arch-kites, but their specification was in glider's models. In 2013 they tested the "Wing 7", a kite with 8 meters of wingspan, 20 kW of rated power and four on-board rotors, with a new idea of bimodal flight to solve take-off and landing issues. In the bimodal flight [27] the device takes off with the wing plane in a vertical position, driven by its propellers thrust. This flight mode is similar to a quadcopter flight and rotors are used as engines. Once all the tether has been unwound, the device changes flight mode, becoming a tethered flight airplane. In this second flight mode a circular flight path is powered

by the wind itself and rotors are used as generators to convert power from the wind. During this phase the cable length is fixed, avoiding the tether fatigue. To land, a new change of flight mode is performed, and he lands as a quadcopter. After previously investing in the company, Google acquired Makani in 2013 and included them in the project X, a research and development facility [5] Makani is currently developing a 600 kW prototype, 'the M600'. The M600 has eight turbines, each with five propeller blades, and has a wingspan of 26 m.

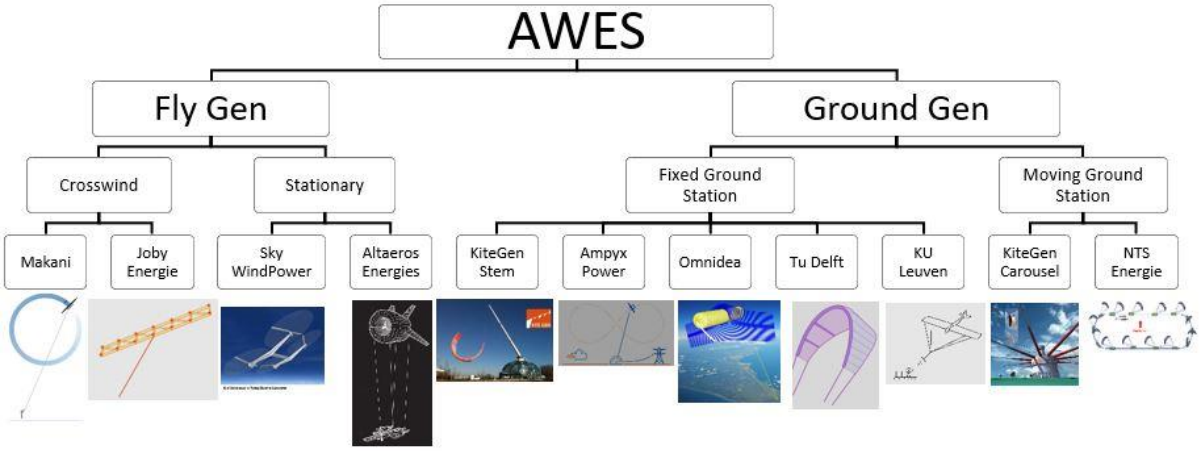

Figure 1.4 Classification of AWES and summary of the different companies/colleges and its prototypes

1.3 Goals and Dissertation Structure

This dissertation goal is to create a numeric model that can predict the power curve and amount of energy produced by a cross wind kite based in Makani's prototype. This model was developed with Simulink and Matlab, based on the equations from Loyd's paper "Crosswind Kite Power" [6] and was analysed the impact of several parameters as wind speed, kite size, tether length, roll angle, orbit amplitude and kite's system of force and compare them with Loyd's paper results.

The following structure was adopted for the organization of work:

- In chapter 2 will be presented the theoretical concepts necessary for a better understanding of the studied subject. This chapter intends to present all the equations system used during the dissertation as the spherical coordinates, system of forces in the kite and tether, kite and wind velocities and power output.

- In chapter 3 will be described the numerical implementation of the equations of chapter 2 in the model created in Simulink and validate the obtained results in agreement with Loyd results.

- In chapter 4 will be presented the case study, the "M600" prototype, created by Makani Power, were will be specified some of its characteristics and will be implemented the model created in chapter 3. This chapter intends to show how much energy this technology would

produce, compare him with the Loyd's results based in the C-5A aircraft and discuss the obtained results

- In chapter 5 will be presented the final conclusions and futures studies that can be made in this area and to complement this MSc dissertation.

Chapter 2. Theoretical Concepts

This chapter is intended to analyse some aerodynamic concepts allowing to posteriorly characterize the kite's motion using Loyd's equation system.

In his model, Loyd compares three power generation models: the relative lift power from a weightless simple kite (F_S) and from a crosswind kite (F_C), and the relative drag power produced by from a crosswind kite (F_D) [6].

Kites behave like an aerodynamic vehicle restrained by a tether, producing lift $\vec{L}$ and drag $\vec{D}$ as they move relative to the air.

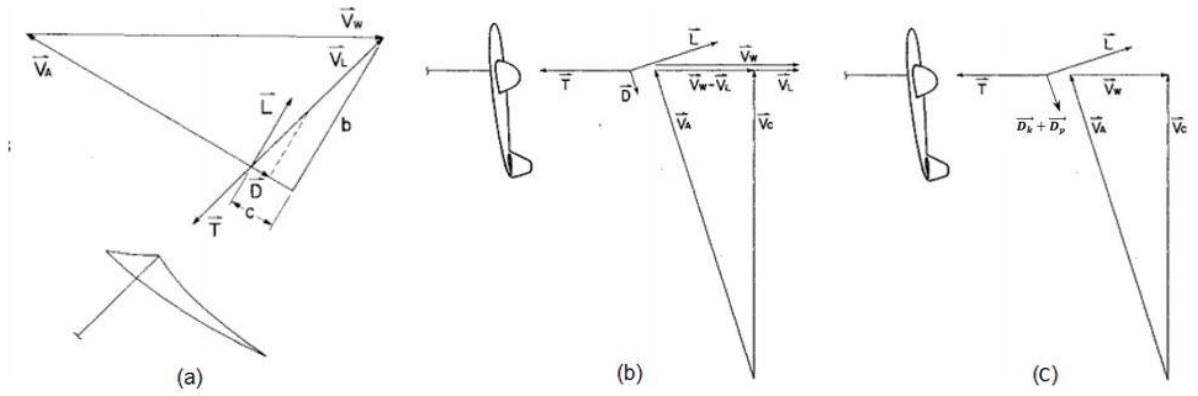

Figure 2.1 Forces and velocities applied on a simple kite (a) and on a crosswind kite (b) both in lift power production and on a crosswind kite in drag power production (c) [6]

The simple kite (Figure 2.1a) faces into the wind, remaining static if the tether is restrained. When the kite is pulled upwind, by a lift force, that acts on the tether to produce power (F_S). That mode of operation is called lift power production. Looking at Figure 2.1a, $\overrightarrow{V_A}$ is the relative kite velocity through air, that is the resulting vector of the wind $(\overrightarrow{V_w})$ and load $(\overrightarrow{V_L})$ velocity vectors, so his magnitude is given by:

$$V_A = \sqrt{{V_L}^2 + {V_W}^2} \tag{2.1}$$

The angle of attack, represents the angle between the kite's chord line (imaginary straight line, joining the leading and trailing edges of the aerofoil) and the flow direction $(\overrightarrow{V_A})$. If this angle is zero, lift is null, in other words, the lift only exists if the angle of attack is greater than zero and for that, the wing profile must be asymmetrical.

The drag $(\vec{D})$, represents the force of resistance to kite's movement, in the opposite direction to the kite's apparent velocity $(\overrightarrow{V_A})$, and perpendicular to $\vec{L}$. $\vec{T}$ is the kite's tether tension that is always in the tether's direction.

In the case of the crosswind kite (Figure 2.1b), the main difference is that the device does not remain static, moving through the air with a velocity $\overrightarrow{V_C}$ which is normal to the wind. Power (F_C) is generated by the load created by lifting the kite. The velocity created by this load ($\overrightarrow{V_L}$) is parallel to $\overrightarrow{V_w}$, so the effective velocity of the wind is reduced to $\overrightarrow{V_w} - \overrightarrow{V_L}$.

Power can also be produced by loading the kite with additional drag (F_D), like is shown in the Figure 2.1c. Air turbines on the wing of the kite result in drag power. In this mode of operation, the tether is not extensible, so his length is always the same. The total drag $\vec{D}$ is the sum of the drag on the kite $\overrightarrow{D_k}$ and the air turbines drag $\overrightarrow{D_P}$, and the velocity created by the load is zero, $\overrightarrow{V_L}$=0.

In the following figure is possible to compare the power output of these three modes of operation:

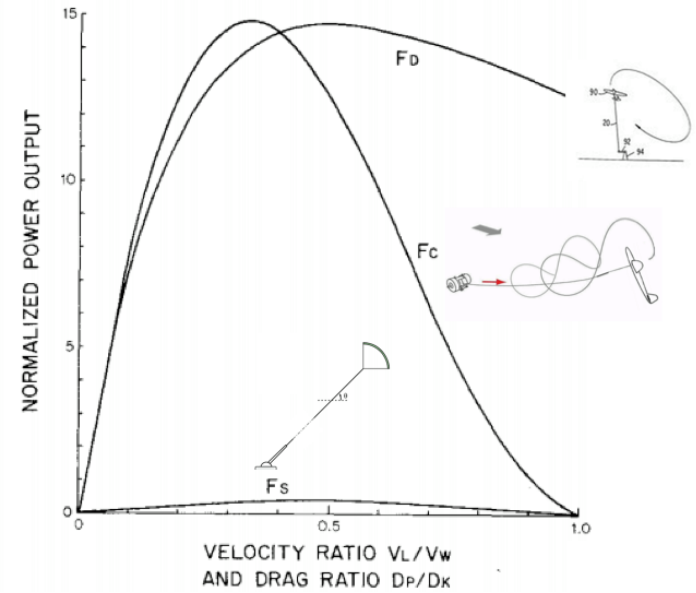

Figure 2.2 Relative power from the different modes of operation with L/D_k of 10 [6]

This last mode of power generation (F_D) is the one that will be studied in this MSc dissertation, which is the mode of operation performed by the M600 prototype.

2.1 Assumptions

In Loyd's paper, some assumptions were made that need to be referred and taken into account throughout this dissertation.

A better understanding of the efficiencies of the kite or the turbine depends on the design details, which are beyond the scope of the paper, so the kite and turbine are assumed to have no losses. Based on that, that assumption has an error between 10 and 20%. The efficiencies of the additional power conversions required to deliver shaft power at the ground were also not considered.

The criteria for the efficiencies of a kite or its turbines are different from those used by Betz. The kite sweeps out an annulus that could be compared to a turbine disk. However, the section occupied in this annulus by the kite is much smaller than the one occupied by the turbine blades and consequently the slowing of the wind is smaller too. In the Betz sense, if this slowdown effect is small, the kite's efficiency will be low. However, the power produced is higher than it would be if the kite were flying in wind that had been more slowed down. Since calculations of kite performance have resulted in Betz efficiencies of a few percentage points, the induced effects of the kite slowing the wind are assumed to be negligible.

The wind was assumed to blow only along the x-axis.

2.2 Equations System

To predict the flight path of the kite it's necessary to define its equations system. To reach this goal, this system was obtained based on Loyd's model [6].

2.2.1 Spherical Coordinates

A spherical coordinate system is a coordinate system for three-dimensional space where the position of a point is specified by three numbers: the radial distance of that point from a fixed origin (R), the polar angle measured from a fixed zenith direction ($\theta - \text{theta}$), and the azimuth angle of its orthogonal projection on a reference plane that passes through the origin and is orthogonal to the zenith ($\emptyset - \text{phi}$), measured from a fixed reference direction on that plane.

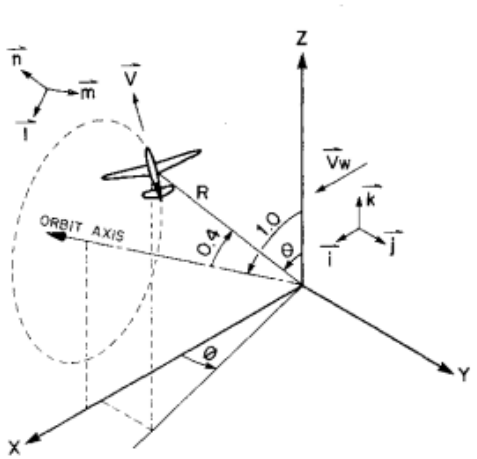

Figure 2.3 Representation of kite's motion, spherical coordinates, velocities components and unit vectors [6]

The Figure 2.3 illustrates the parameters allowing the characterization of the kite's motion which will be defined further ahead in this dissertation.

2.2.2 Velocities

In Loyd's paper, the velocity of the kite, also called ground speed, is defined as:

$$\vec{V} = R\left(\dot{\theta}\,\vec{l} + \dot{\emptyset} sin\theta \vec{m}\right) \tag{2.2}$$

And assuming that wind only blows along the abscissa axis, so:

$$\vec{V_w} = V_w\left(cos\theta cos\emptyset \vec{l} - sin\emptyset \vec{m} + sin\theta cos\emptyset \vec{n}\right) \tag{2.3}$$

The important quantity in the generation of lift is the relative velocity between the object and the air, also called airspeed. Airspeed cannot be directly measured from a ground position, it must be computed from the ground speed and the wind speed. Airspeed is the vector difference between the ground speed and the wind speed [28]. Once $\vec{V_w}$ and $\vec{V}$ are defined in the coordinate system (l, m, n), the velocity of the kite through the air (airspeed) $\overrightarrow{V_A}$ comes:

$$\vec{V_A} = V_l\,\vec{l} + V_m\,\vec{m} + V_n\,\vec{n} \tag{2.4}$$

Where,

$$V_l = R\dot{\theta} - V_w cos\theta cos\emptyset \tag{2.5}$$

$$V_m = R\dot{\emptyset}\, sin\theta + V_w sin\emptyset \tag{2.6}$$

$$V_n = -V_w sin\theta cos\emptyset \tag{2.7}$$

2.2.3 System of Forces

The acceleration of the kite is determined by four forces: tether tension $\vec{T}$, weight $\vec{W}$, lift $\vec{L}$ and drag $\vec{D}_k$, as shown in the next figure:

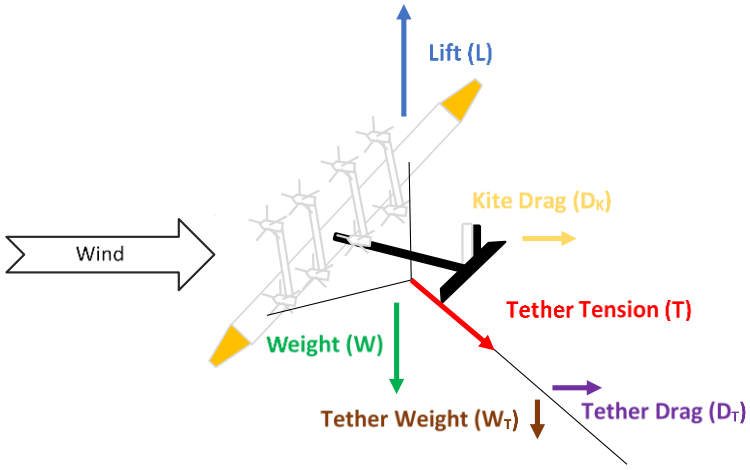

Figure 2.4 Forces actuating on the system

Assuming the gravity in the -z direction only, the weight of the kite is:

$$\vec{W} = W(sin\theta\ \vec{l} - cos\theta\ \vec{n}) \tag{2.8}$$

The drag is opposite in the direction of $\vec{V_A}$, so is defined as:

$$\vec{D}_K = -\frac{1}{2}\ \rho\ C_D\ A_k\ \vec{V}_A \sqrt{V_l^2 + V_m^2 + V_n^2} \tag{2.9}$$

where ρ is air density (1,225 kg/m^3), C_D is the kite drag coefficient and A_k is wing reference area of kite.

To maintain a precise orbit, the flight path must be controlled by the variation of the tangent of roll angle (C), which is further defined.

It's convenient to define the factor H, to simplify the calculations:

$$H = \sqrt{(1 + C^2)\ (V_l^2 + V_m^2)} \tag{2.10}$$

The direction of the lift $\vec{L}$ has two components while on a turn, each one normal to $\vec{V}_A$, in agreement with the definition of lift. One is in the plane of $\vec{V}_A$ and $\vec{n}$ (L') and the other is normal to this plane (F_C), as shown in the next figure:

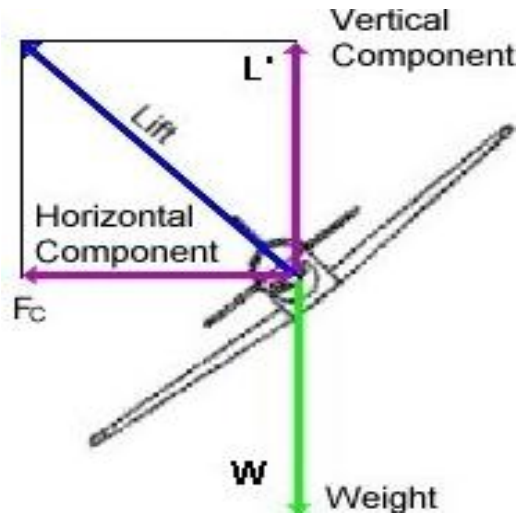

Figure 2.5 Lift components and weight applied on the kite in a turn [29]

Taking that into account, lift becomes:

$$\vec{L} = \left\{\frac{1}{2}\,\rho\, C_L\, A_k\, V_A / \sqrt{(1+C^2)\,(V_l^2+V_m^2)}\right\}\left[-\,(V_l V_n + V_m V_A C)\vec{l} - \,(V_m V_n - V_l V_A C)\vec{m} + \left(V_l^2+V_m^2\right)\vec{n}\right] \qquad (2.11)$$

where C_L is the kite lift coefficient.

The tether tension is in the negative $\vec{n}$ direction only (see Figure 2.3). Thus,

$$\vec{T} = -\left[W\left\{\frac{\left(R^2\dot{\theta}^2 + R^2\dot{\phi}^2\, sin^2\theta\right)}{(gR)} - cos\theta\right\} - 1/2\rho\, C_L\, A_k\, V_A\left\{\frac{V_n}{L/D} - \frac{(V_l^2+V_m^2)}{H}\right\}\right]\vec{n} \qquad (2.12)$$

g represents the acceleration of gravity (9,8 m/s^2) and D the total drag.

It's now possible to define the acceleration components:

$$\ddot{\theta} = \dot{\phi}^2 \sin\theta\cos\theta + \frac{g\sin\theta}{R} - \frac{gC_L\rho A_k V_A}{2WR} \times \left(\frac{V_l}{L/_D} + \frac{V_l V_n - V_m V_A C}{H}\right) \qquad (2.13)$$

$$\ddot{\phi} = \frac{-2\dot{\theta}\dot{\phi}\cos\theta}{\sin\theta} - \frac{gC_L\rho A_k V_A \sin\theta}{2WR} \times \left(\frac{V_m}{L/_D} + \frac{V_m V_n - V_l V_A C}{H}\right) \qquad (2.14)$$

Once the four forces are defined, the total acceleration of the kite comes:

$$\vec{a} = R\left(\ddot{\theta} - \dot{\phi}^2 \sin\theta\cos\theta\right)\vec{l} + R\left(\ddot{\phi}\sin\theta + 2\dot{\theta}\dot{\phi}\cos\theta\right)\vec{m} - R\left(\dot{\theta}^2 + \dot{\phi}^2\sin^2\theta\right)\vec{n} \qquad (2.15)$$

The tether must be strong enough to provide the tension given in equation 2.12. When this tether tension is equal to the strength of the cable, the weight of the tether is:

$$W_T = gRT\rho_T/\sigma \tag{2.16}$$

ρ_T is the tether density and σ is the tether working stress (Pa). Working stress is the maximum allowable stress that a material may carry.

Since the part of the tether near the kite moves faster than the part near the ground, the drag load produced by the tether on the kite is evaluated by integration of the incremental moment created by the tether drag over the length of the tether. Assuming the tether reference area to be $4R\sqrt{A_T}$, where A_T is the tether cross-sectional area, the resulting drag of the tether is:

$$D_T = \frac{1}{2}\rho C_{DT} R\sqrt{T/\sigma}\, V_A^2 \tag{2.17}$$

C_{DT} represents the tether drag coefficient.

2.2.4 Power Drag

As previously mentioned, power can be produced by on-board air turbines that create drag. Looking at Figure 2.2, the maximum value of F_D occurs at 0.5 D_P/D_k. Considering the tether's drag, the power drag comes:

$$D_P = 0.5\ (D_K + D_T) \tag{2.18}$$

Since total drag is the sum between D_P, D_K and D_T, comes:

$$D = 1.5\ (D_K + D_T) \tag{2.19}$$

This means that on-board turbines increase the total system drag by 50%.

It's known that power is the amount of energy transferred per unit time, defined in the SI units by joules per second (J/s) recognised as Watt (W). In other words, power is the rate of doing work expressed by:

$$P = \frac{dw}{dt} \tag{2.20}$$

The work (w) is a force F applied over a distance r, so:

$$w = F \times r \tag{2.21}$$

So, equation 2.20 can be rewritten as:

$$P = \frac{d}{dt}(F \times r) = F \times \frac{dr}{dt} = F \times V^{1} \tag{2.22}$$

Neglecting turbine losses, the power produced by air turbines adding a drag D_P, to the kite moving through the air at V_A is:

$$P = D_P \times V_A \tag{2.23}$$

[1] In this particular case, V is representative of a common velocity and not the kite velocity

Chapter 3. Numeric Implementation

In a preliminary stage of a project, it is very important to use tools that gives us the chance to test several solutions and to predict (and overcome) some problems that may exist in the future. Nowadays, there are plenty of computer simulation which programs makes this possible, and in this dissertation, the program chosen to simulate the crosswind kite behaviour was Simulink version 8.5, an extension of MATLAB R2015a.

In the next subchapters will be described the numeric implementation of the model in Simulink/MATLAB.

3.1 Initial Conditions

As first approach, as it shown in Loyd's paper [6], it was created a model based on a C-5A aircraft (Figure 3.1), a large military transport aircraft with 68 meters of wingspan [30].

Figure 3.1 C-5A model aircraft [31]

In Loyd's paper, he studied three examples of large-scale power production, resumed on Table 3.1:

Table 3.1 Examples of Loyd's article calculations

	Example	I	II	III
Kite	Wing area (m^2)	576	1000	2000
	Lift-to-drag ratio	20	40	40
	Strength-to-weight ratio	10	10	10
	Coefficient of lift	1	1	1
Tether	Length (m)	400	1200	1200
	Working stress (MPa)	345	345	345
	Density (Mg/m^3)	8	8	8
	Coefficient of drag	0.04	0.04	0.04
Wind	Speed (m/s)	10	10	10
Results of calculation	Average power output (MW)	6.7	19	45
	Peak tether tension (MN)	3.2	10.6	22.2

The kite and tether's parameters, of example I, were applied in a Matlab's model which recognize them as constants in his algorithm (see Attachment 1). The tether's coefficient of drag is a fairly undersized value for a circular cylinder shape, however since the tether shroud need not produce lift [6], that value was approximated to the drag coefficient of a streamlined body . To verify the model, the final results must approach to average power output and peak tether tension of example I, which are 6.7 MW and 3.2 MN, respectively.

3.2 Simulink Model

Simulink, developed by MathWorks, is a graphical programming environment for modelling, simulating and analysing multidomain dynamic systems. Simulink is integrated with MATLAB, enabling the user to incorporate MATLAB algorithms into models and export simulation results to MATLAB for further analysis. This program is widely used in automatic control and digital signal processing for multidomain simulation and Model-Based Design (MBD). MBD is a mathematical and visual method of addressing problems associated with designing complex control, signal processing and communication systems. Rather than using complex structures and extensive software code, designers can use Model-based design to define plant models with advanced functional characteristics using continuous-time and discrete-time building blocks [32].

This blocks model was created with the equations system defined in chapter 2 and was structured with blue blocks that represents subsystems of the main system, that will be described more detailed below (see Attachment 2).

3.2.1 Spherical Coordinates

This subsystem is the base for this model implementation, once as anticipated in the chapter 2.2.1, the spherical coordinates definition will allow the prediction of the kite's motion in three-dimensional space.

The kite flight path is circular about an orbit axis directly downwind from the anchor point, one radian down from the z axis and 0.4 radians up to orbit axis. To define this, it was considered the time function of the angular position of a uniform circular motion:

$$\beta = \beta_0 + \dot{\beta}_0 . t \tag{3.1}$$

Where β_0 is the initial position of the kite, and $\dot{\beta}_0$ his derivative given in radians per second. As a first aproximation, $\beta_0 = 0\ rad$ and $\dot{\beta}_0 = 3\ rpm\ \left(\frac{\pi}{10}\ rad/s\right)$, which means that the kite gives a full rotation in 20 seconds. It was considered that β is zero in the highest position (when the altitude is maximum) and the kite moves in counter-clockwise direction, so β increases in this way as shown in Figure 3.2.

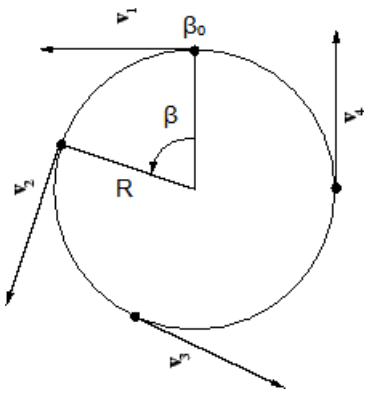

Figure 3.2 Representation of the Beta parameter

To define the spherical coordinates it was used the Rodrigues's formula rotation [33], an efficient algorithm for rotating a vector in a 3D space, given an axis (u) and angle of rotation (φ) defined by:

$$v_{rot} = v\cos\varphi + (u \times v)\sin\varphi + u(u \cdot v)(1 - \cos\varphi) \tag{3.2}$$

v is a vector in $\mathbb{R}^3$ and u is a unit vector describing an axis of rotation about which v rotates by an angle φ according to the right hand rule. In this case, u is the vector represented in Figure 2.3 by *orbit axis* that is defined in the spherical coordinate system by [1 1 0]; v is the vector defined by spherical coordinates [R θ $\emptyset$]; and φ is the angle of rotation defined by β in equation 3.1. $(u \times v)$ and $(u \cdot v)$ are, respectively, the cross and the dot product between v and u vectors.

To apply equation 3.2, was used the "MATLAB Function" block, presented in Simulink library. This block allows the inclusion of a Matlab function in the Simulink model, where is necessary to specify its inputs and outputs. In this case, the input is β which is already defined in Simulink model, and the return values (outputs) are the spherical coordinates (v_{rot}). u and v are specified in block editor, where v must be defined as the first position of the kite, when $\beta = 0$, that is [400 0.6 0]. The desired v_{rot} must be in the form of spherical coordinates (R,θ,$\emptyset$), however to use the Rodrigues formula, these must be in cartesian coordinates (x,y,z) so is necessary to use the coordinate systems conversions [34]:

Table 3.2 Coordinate systems conversions

Spherical to Cartesian	Cartesian to Spherical
$x = R\sin\theta\cos\emptyset$	$R = \sqrt{x^2 + y^2 + z^2}$
$y = R\sin\theta\sin\emptyset$	$\theta = \cos^{-1}\left(\frac{z}{\sqrt{x^2 + y^2 + z^2}}\right) = \cos^{-1}\left(\frac{z}{R}\right)$
$z = R\cos\theta$	$\emptyset = \tan^{-1}\left(\frac{y}{x}\right)$

The output, v_{rot} gives a three columns matrix, where the first one is the radial distance (R) which is a constant value, and the second and third columns are respectively the polar (θ) and azimuth angles ($\emptyset$) obtained for each value of β.

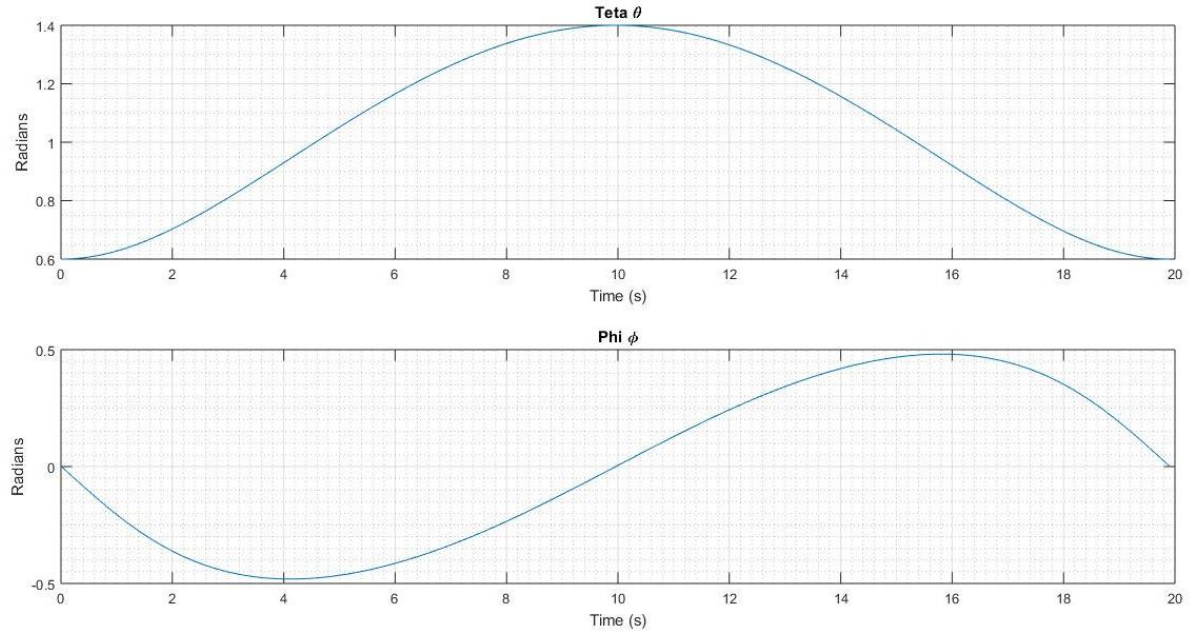

Figure 3.3 Spherical coordinates representation for 3 RPM in one cycle of rotation (20 seconds)

Based in Table 3.2, is possible to convert these spherical to cartesian coordinates, that allows to know strictly the spatial position of the kite. The block "Derivative" of Simulink, allows to obtain the time derivative of spherical $\left(\frac{d\theta}{dt}, \frac{d\emptyset}{dt}\right)$ and cartesian $\left(\frac{dx}{dt}, \frac{dy}{dt}, \frac{dz}{dt}\right)$ coordinates which are used in equations 2.2, 2.5, 2.6, 2.12, 2.13, 2.14 and 2.15 with the notation of $\dot{\theta}$ and $\dot{\emptyset}$. Is possible to export the values of spherical coordinates and his derivatives to MATLAB editor with the "To Workspace" block and draw a three-dimensional representation of the kite flight path and his velocity, with "plot3" and "quiver3" respectively, commands of MATLAB.

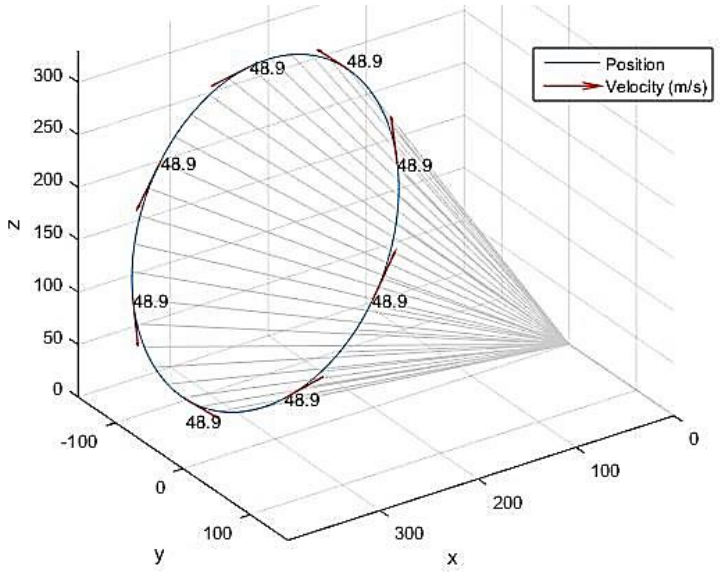

Figure 3.4 Position and velocity of the kite for 3 RPM

3.2.2 Velocities and Wind Model

This subsystem block has the purpose of calculate the kite velocities by application of equations 2.2, 2.4, 2.5, 2.6 and 2.7. To insert these and all the equations of Chapter 2.2 in the Simulink model, was used the "Fcn" block, which applies the specified mathematical expression to its inputs. The inputs, equations and outputs of this subsystem are illustrated in Figure 3.5:

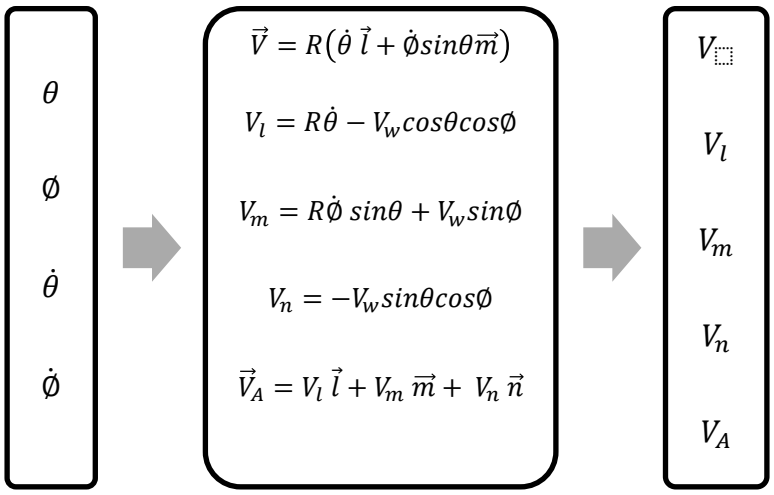

Figure 3.5 Representation of the block "Velocities" operation

To obtain these values is necessary to estimate the wind speed (equation 2.3). In a first approximation, like in Loyd's paper, it was considered the constant value of 10 m/s for V_w, then it was considered a wind model to estimate his variation with the altitude in the atmospheric boundary layer (ABL). The ABL is the part of troposphere that is directly influenced by the Earth's surface presence and responds to this influence with a time scale of about an hour or less. The air layer above the ABL is called the free atmosphere. The ABL depth is quite variable, but it's generally below 2 to 3 km [35]. The diurnal variability and the high frequency of turbulence near the ground are characteristics that distinguish the ABL from the rest of the atmosphere.

The mean velocity profile of a turbulent atmospheric boundary layer can be obtained by two ways [36]:

By the Prandtl's logarithmic law, commonly called wall law, which can be described as:

$$U(h) = \frac{u_*}{k} ln\left(\frac{h}{h_0}\right) \tag{3.3}$$

where u_* is the friction velocity in the ground, k is the universal Von Kármán constant, h is the height and h_0 is the surface roughness length;

Or by a power law assumption, which allows the calculation of speed values from a reference value:

$$\frac{U(h)}{U_{ref}} = \left(\frac{h}{h_{ref}}\right)^{\alpha} \tag{3.4}$$

where U_{ref} is the velocity of wind at the height of h_{ref} and α is a parameter which varies in function of the surface roughness.

To obtain the wind profile it was used the equation 3.4 instead of equation 3.3, because it's difficult to predict the ground friction velocity (u_*). The α parameter was defined as 1/7, typical of mostly flat

surfaces with little roughness (excluding water, snow and ice), like the locals where this system will operate [37]. Based on a 2000 study carried out by Cristina L. Archer and Mark Z. Jacobson, they concluded that locations with appreciable wind power potential (class ≥ 3[2]), can register a mean V_{10} (wind speed from an elevation of 10 m) of 6,50 m/s at onshore stations [2]. With these values and in consistency with the wind speed of 10 m/s considered in Loyd's paper, it is possible to obtain the corresponding height, by applying equation 3.4, which gives a value of 204 m, a consistent value taken into account the kite mean altitude (Figure 3.4). Resorting again to equation 3.4, it is possible to construct the wind model for this situation, knowing that h is the altitude of the kite which is given by the multiplication of $cos\theta$ for the tether length (see Table 3.2).

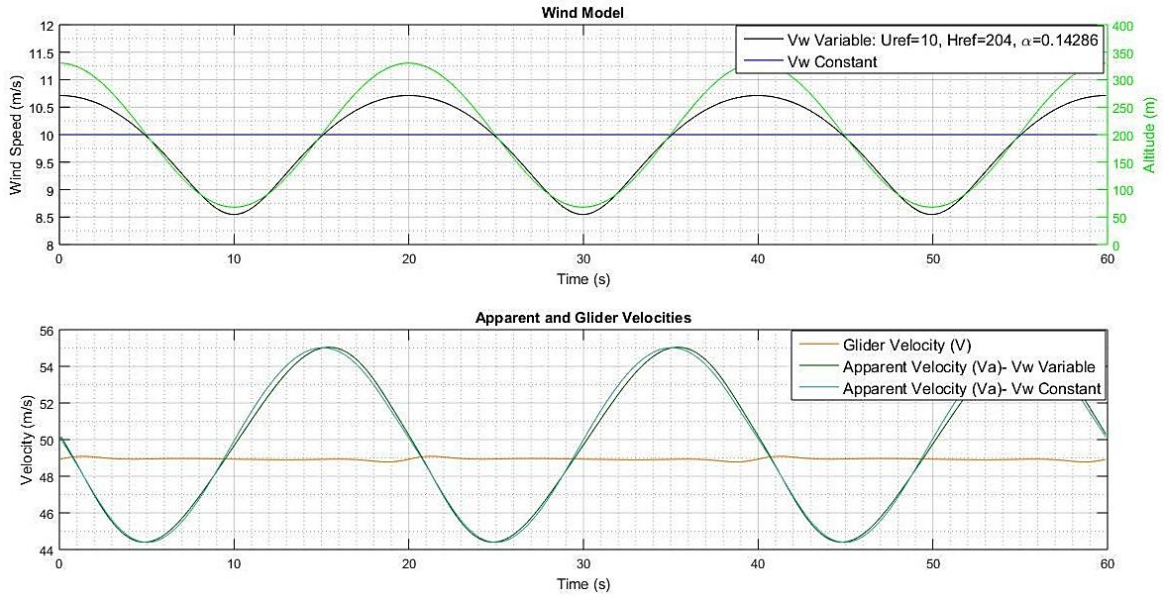

Figure 3.6 Graphic representation of wind model and his corresponding altitude (top graph) and kite and apparent velocities (bottom graph) to 3 RPM

In the first plot of Figure 3.6 is possible to observe, as already mentioned in chapter 1.1, that the growth and decrease of the wind speed (black line) is proportional to the altitude (red line). This graph also intends to show the contrast between the two models used to represent the wind variation: assuming the wind constant (neglecting the wind boundary layer effect - blue line) and variable (black line). In the graphic below is possible to see that V (orange line) and V_A (cyan and green lines) both have a much greater magnitude than V_w, and as previously noted $V_A = V - V_w$. Then it is predictable that wind velocity does not cause much variation in V_A, whether constant or variable given the range of altitudes seen by the kite and the boundary layer conditions assumed. Also, since in this model the speed of rotation is being enforced, the speed of the kite (V) is approximately constant (orange line).

[2] At a specified height above the ground, each class represents a range of mean power density (W/m^2), with class 1 winds containing the least energy and class 7 winds containing the most energy. Each class has equivalent wind speed ranges, but these are dependent on the height at which the wind map is referring. In this dissertation the class is referred to a height of 80 meters.

3.2.3 Roll Angle Variation

One of the challenges with using a kite type system for extracting wind energy is his susceptibility to gusts and turbulence, in other words, variations in the wind speed can disturb the system significantly, causing it to enter into an unrecoverable spin or dive. It's important to be able to establish whether the system is capable of following a desired trajectory determined in the presence of variations in the wind speed around the mean. Then, it is necessary to stablish some kind of control to maximize the generated energy. In Loyd's paper the control action is guaranteed by the tangent of roll angle figured by C letter, which is not defined in the paper, so it is necessary to characterize it.

The roll angle is the rotation operation performed around the longitudinal axis of the kite [38]. Positive angles correspond to the starboard (right) wing lowered below the horizontal plane, that leads the kite to fly to the right and negative angles corresponds to the opposite like illustrated in Figure 3.7.

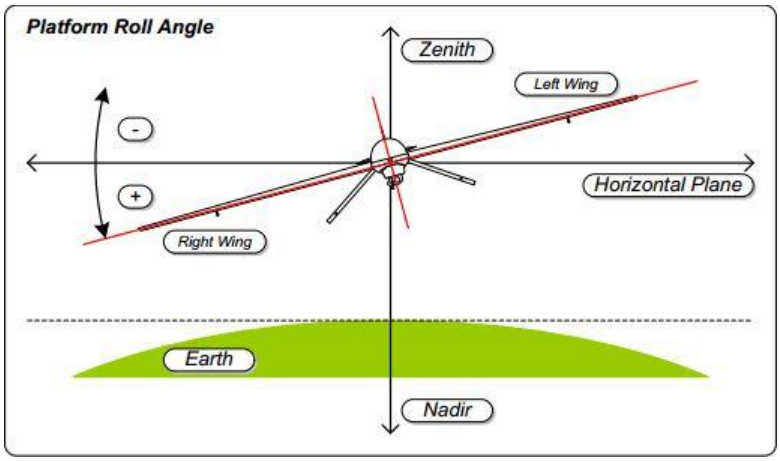

Figure 3.7 Variation of roll angle about the kite horizontal plane [39]

To get an approximation of C, the equation 2.14 was used, which gives the second order derivative of the spherical coordinate $\emptyset$, that was already calculated. Looking at Figure 3.3, $\emptyset$ has three roots. These three points corresponds to the positions $\beta = 0, \pi$ and 2π but as representative of a looping motion the first and last positions represent the same. By definition, the second derivative has the same roots of his own function, so equating equation 2.14 to zero and solving in order to C it's possible to obtain his values for the positions of $\beta = 0$ and π. To help with this calculation, the function "*fzero"* of Matlab was used. In the sides ($\beta = {}^{\pi}/_{2}$ and ${}^{3\pi}/_{2}$) the roll angle was assumed to be zero (C=0), when the kite is directly downwind and upwind. In the next figure is possible to see the value of the roll angle in each one of these positions.

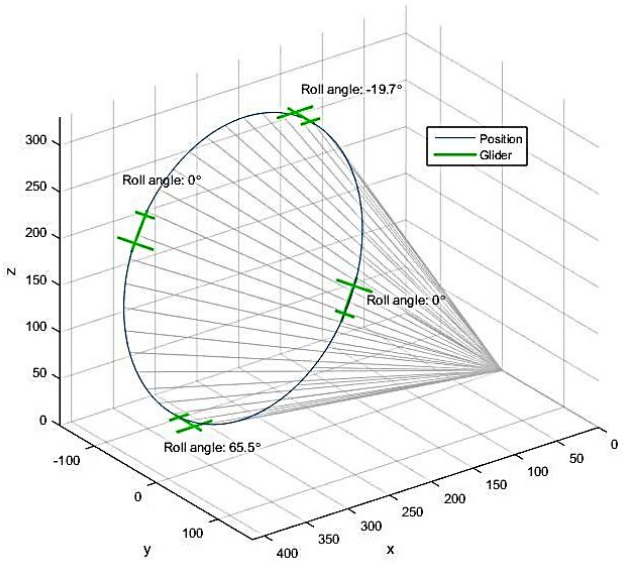

Figure 3.8 Representation of the kite position and the respective values of roll angle in four positions for 3 RPM

The obtained results for the roll angle are in agreement with the flight path of the kite: the negative roll angle lifts the right wing and lowers the left wing and the kite descends to the left, the positive angle lowers the right wing and lifts the left wing and the kite ascends to the left. Knowing these four positions, it's now possible to create a linear variation to make an approximation of the roll angle behaviour (Figure 3.9) given by the next expression:

$$Roll\ angle\ (\beta) = \left[\frac{Roll\ angle(\beta = 0) + Roll\ angle(\beta = \pi)}{2}\right]\cos^2\beta - \left[\frac{Roll\ angle(\beta = \pi) - Roll\ angle(\beta = 0)}{2}\right]\cos\beta \qquad (3.5)$$

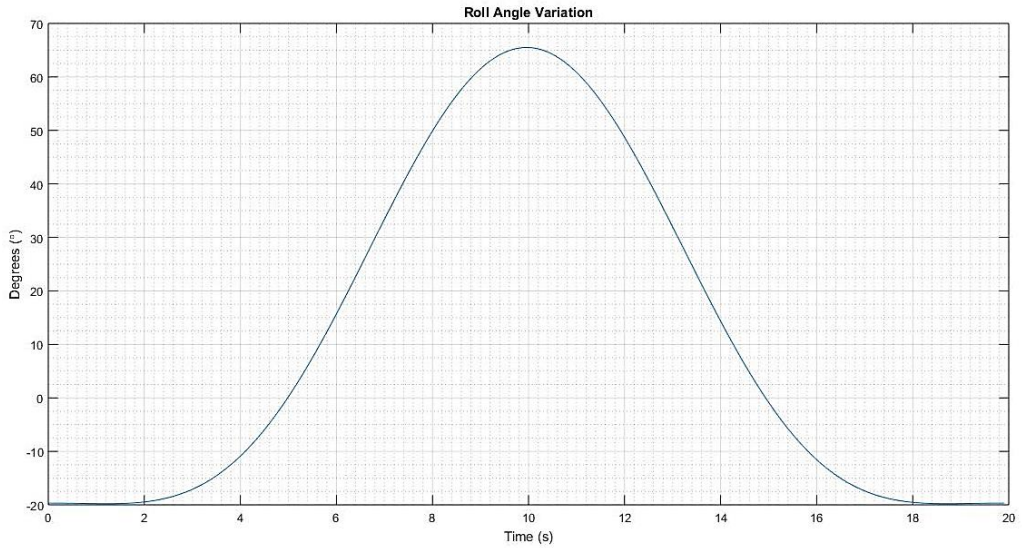

Figure 3.9 Roll angle variation for 3 RPM to one cycle of rotation (20 seconds)

And finally, C is given by:

$$C(\beta) = \tan[Roll\ angle(\beta)] \tag{3.6}$$

Looking at the previous equation is not clear its relationship with the turbulence and with variations in the wind speed. To ensure this kind of control, a more elaborate controller would be needed, based in new technology, that can control the kite's flight path in its six degrees of freedom (6DoF).

3.2.4 System of Forces

3.2.4.1 On Kite

This subsystem block has the purpose of obtaining the results of equations 2.8, 2.9, 2.11 and 2.12. The goal of this subsystem is illustrated in the next figure:

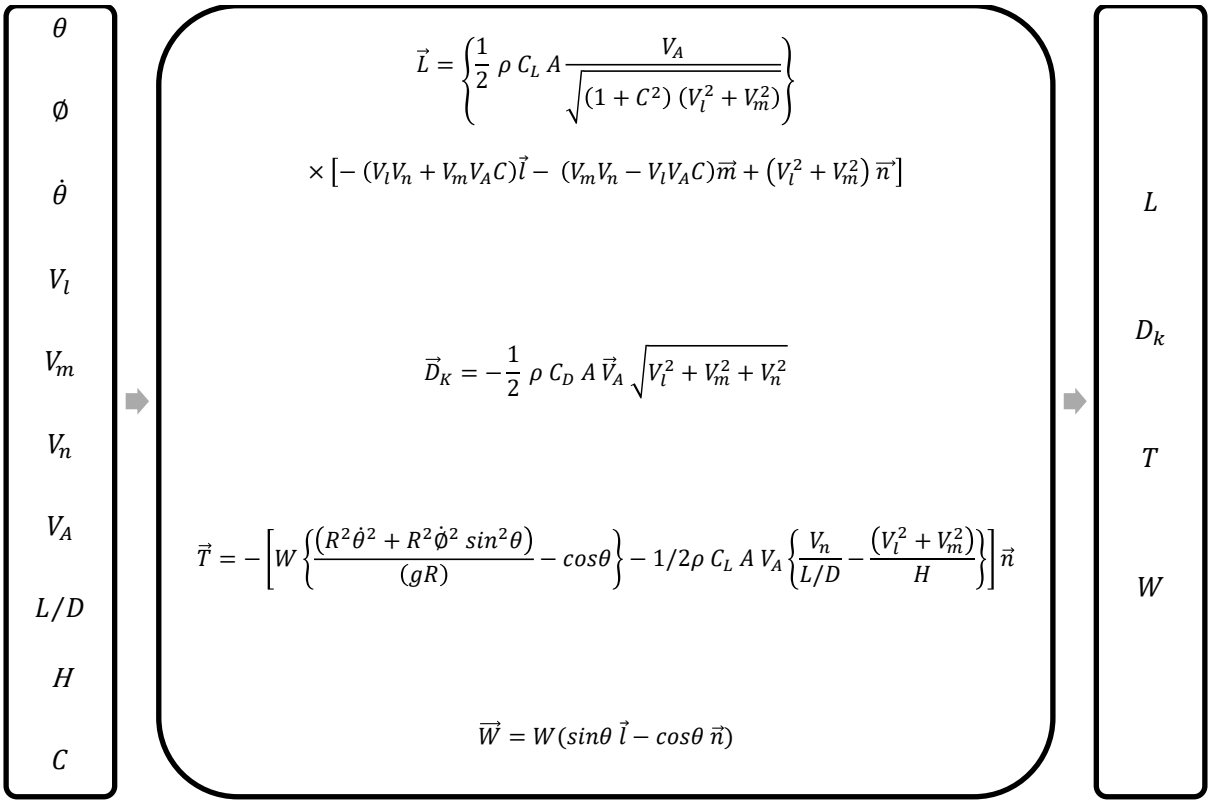

Figure 3.10 Representation of the block "Forces on Kite" operation

In this model, *W* corresponds to C-5A weight which is given by the product between the aircraft mass and the gravity acceleration. This aircraft weighs about 233 tons [30] and the gravity acceleration has conventionally the value of 9.8 m/s^2, which gives a weight of approximately 2.28 MN.

3.2.4.2 On Tether

This subsystem block has the purpose of obtaining the results of equations 2.16 and 2.17. The goal of this subsystem is illustrated in the next figure:

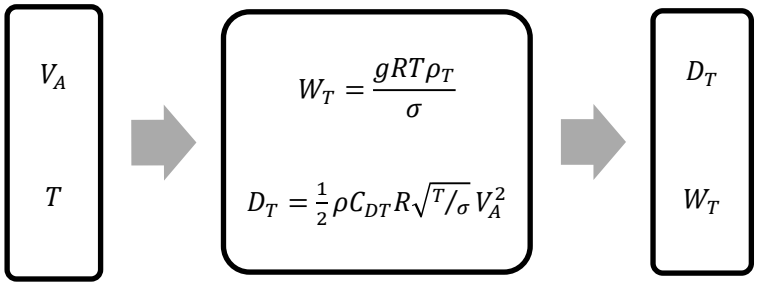

Figure 3.11 Representation of the block "Forces on tether" operation

T/σ is the transversal area of the tether, once is the division of a force by a pressure, that by definition gives an area (m^2), so is possible to obtain the tether diameter equating this to πr^2, being r half of the tether diameter, which becomes:

$$d = 2 \times \sqrt{\frac{T}{\sigma \times \pi}} \tag{3.7}$$

Replacing T and σ with the values of Table 3.1 (example I), that are 3.2 MN and 345 MPa respectively, is possible to obtain a diameter of approximately 11 cm, which gives an idea of the tether thickness.

3.2.5 Acceleration

In this subsystem block, the acceleration and its components are calculated based on the equations 2.13, 2.14 and 2.15. The goal of this subsystem is illustrated in the next figure:

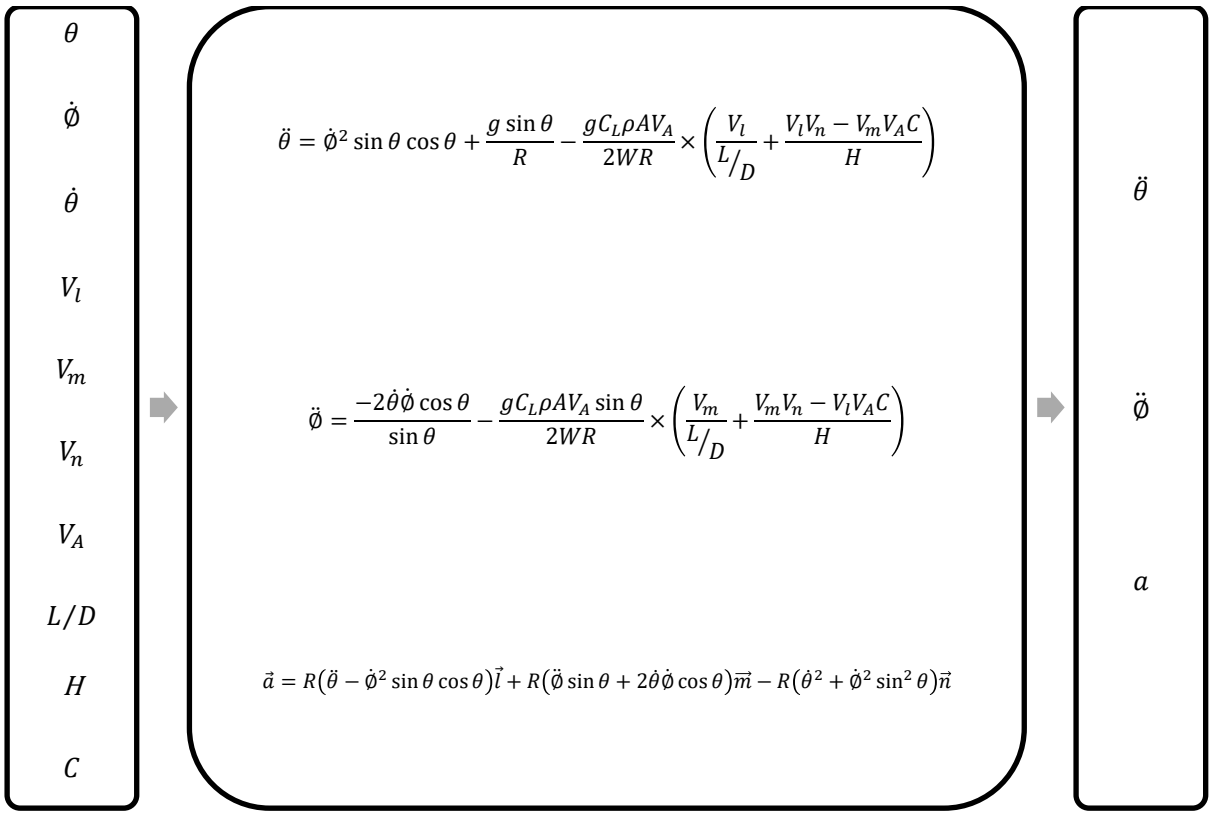

Figure 3.12 Representation of the block "Acceleration" operation

3.2.6 Power Output and Model Verification

With the last subsystem of this model called "Power Output", it is possible to obtain the power curve of the tethered system by applying of equation 2.23. This model was simulated for one orbit cycle with a fixed step of 0.1 seconds based in the Bogacki-Shampine solver which is a default of the program.

As referred before, to verify the model, the final result must approach to the average power output and peak tether tension of example I of Table 3.1. For this purpose, several tests were made, for different RPM ($\dot{\beta}_0$) and wind speed (constant or variable) values and the relative error between the measured values and those obtained by Loyd, was calculated. The final results are summarized on the next table:

Table 3.3 Simulations results for each RPM, and windspeed variable and constant and comparation with Loyd's results

	RPM=3 (One orbit cycle: 20s)		RPM=5 (One orbit cycle: 12s)		RPM=5.5 (One orbit cycle: 10,91s)		RPM=6 (One orbit cycle: 10s)		RPM=8 (One orbit cycle: 7,5s)		Loyd's Paper
	Vw Constant	Vw Variable	Vw Constant	Vw Variable	Vw Constant	Vw Variable	Vw Constant	Vw Variable	Vw Constant	Vw Variable	Vw Constant
Peak tether tension (MN)	1.347	1.350	2.161	2.040	2.581	2.390	3.086	2.9	4.855	4.330	3.200
Relative error (%)	57.91	-	32.47	-	19.34	-	3.56	-	51.72	-	0
Av. power output (MW)	1.138	1.136	5.037	5.033	6.680	6.674	8.701	8.695	20.850	20.830	6.700
Relative error (%)	83.01	-	24.82	-	0.30	-	29.87	-	211.19	-	0
Tether's thickness (cm)	7.05	7.06	8.93	8.68	9.76	9.39	10.67	10.35	13.39	12.64	10.87

In order to compare the obtained results with those obtained by Loyd, is necessary to take into account the same conditions, so the right velocity of rotation must be chosen when the windspeed has a constant value of 10 m/s, reason why the relative error is only calculated in those cases.

Looking at the previous table is possible to verify that 3 RPM, chosen at a first place, isn't a good approximation for the velocity of rotation of the study case, with high relative errors shown discrepancy between the values. For 8 RPM the discrepancy is even higher, with relative errors bigger than 100%. After making the test for 5 and 6 RPM became obvious that the best result lies in a range between these values, so was made an intermediate test for 5.5 RPM. Therefore, observing the results in its overall, the chosen velocity was 5.5 RPM, where the result of the average power output gets very close to the desired one, with a relative error inferior to 1% and the peak tether tension with a relative error of 19%. It's interesting to see that the tether's thickness increases with the growth of the tension, by application of equation 3.7, which leads to the conclusion that higher tensions require stronger tethers.

To approximate the results to the reality, the wind model described in sub-chapter 3.2.2 was applied, and its results are presented also in Table 3.3, so the model created with these conditions is the chosen one as representative of the kite's flight path and his graphs and results are presented in the attachments (see Attachment 3 and Attachment 4). In the next chapter this model will be applied to the study case, the Makani prototype.

Chapter 4. Study Case

In this chapter will be analysed with more detail, the model "M600" of the Makani Power company, to realize what is its energy potential. With this propose, the model created in Chapter 3, based on a C-5A aircraft, will be now calculated with M600 characteristics.

4.1 Makani Power Prototype

Makani Power the Californian company, founded in 2006 by Corwin Hardham, Don Montague and Saul Griffith, was created with the goal of developing a low-cost renewable energy solution using kite technology [26]. After many years testing several prototypes, in 2016 they finish their first commercial scale system, a kite called "M600" with a rated power of 600 kW and 26 meters of wingspan (see Figure 4.1).

Figure 4.1 Makani's prototype- M600 [40]

As seen in the previous figure, this prototype has eight turbines mounted along the wings, each drives a permanent magnet motor/generator that generates electricity on-board, when they are crossed by airflow. Direct-drive generator units of high power density are supported by the strength and aerodynamic leverage of its wings. The wing is made by a composite material which includes e-glass in its skin and carbon fibre in the spar, a high tensile strength and low weight material, which favour the kite flight manoeuvres due to L/D ratio. For airplanes, this ratio is also referred to as the gliding number, it describes how faster a kite without propulsion can move horizontally compared to its vertical sink rate. The material properties of the tether are important as a tether needs to withstand strong tensions due to high velocity winds. A high voltage tether is required to transmit the electricity to ground level, although the tether weight is an important constraint which could increase the load on the kite. For their

prototype, M600 tether is made in pultruded carbon fibre with a working stress of 2137 MPa and a density of 1760 kg/m^3 [41] which is 6 times stronger, and 4 times less dense than steel used in Loyd's model. The voltage conductor is aluminium, which because its low electrical impedance ensure that the power lost along the tether is minimal. This tether with 440 meters length, allows the kite to reach altitudes between 140 to 310 meters.

The kite takes off from the ground station with the wing plane in a vertical position, driven by the turbine rotors that are used as propellers, like a quadcopter. Once the tether is all unwinded, the device changes flight mode becoming a tethered flight fully autonomous airplane, describing a circular flight path powered by the wind, which is restricted by the tether length. In this flight mode the turbine rotors work as generators to convert power from the wind that is transmitted to the ground station by the conductor tether. In order to land the kite, a new change of flight mode is made, and the device returns to the ground station as a quadcopter. During the take-off and landing phases the device consumes energy, a minimal fraction of the energy which is produced in the autonomous flight mode. In the next figure is summarized the operation of M600 device:

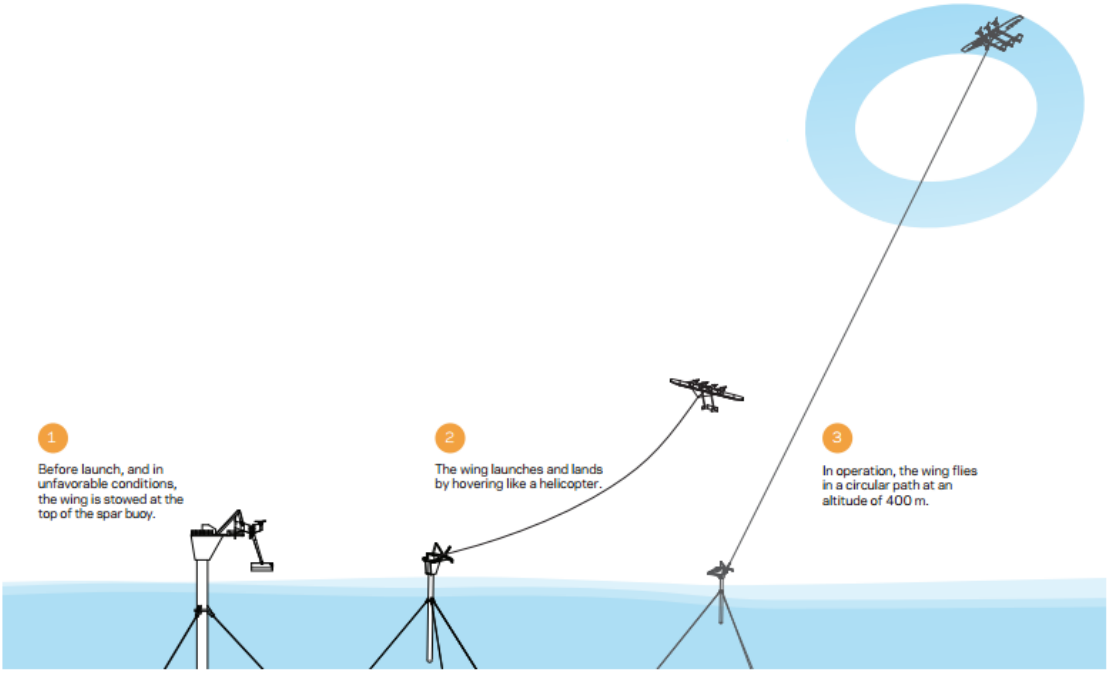

Figure 4.2 M600 bimodal flight [42]

The potential failure of either the device or the tether must be considered in regard to ground safety. In case of the device failure, such as rotor failure due to mechanical malfunctions, the worst scenario is that the radius of influence will be the tether length, so at least one tether length must be guaranteed as safety perimeter. In the case of a fatal tether failure, the M600 on-board generating systems could land safely with the use of their rotors as a quadcopter, given that there is energy storage available otherwise the device could float away. Makani has implemented a supervisory control and data acquisition system that will control and monitor the health of the device including sensors to detect impendence in individual sections of the tether [43]. There are also, regulation and safety procedures which need to be fulfilled, so Makani is committed to working with the Federal Aviation Administration (FAA) of USA to open a safe AWES farm for the operation of several devices. In a

response to FAA [42], they explain how they expect to ensure the safety of its devices and some upcoming tests that need to be done as the operation at night, over long periods of time (weeks, months) and up to 610 meters above ground level and study multiple system farm environments. In this response they specify some characteristics of M600 which will be useful to the next subchapter as the wing area of 35 m^2, the coefficient of lift of 2 and the wing mass of 1050 kg.

4.2 Numerical Implementation

In this subchapter is intended to compare the new inputs for the model created in chapter 3 and compare them with the Loyd's values so then shown their outputs. This comparison is shown in the next table:

Table 4.1 Comparation between C-5A aircraft and Makani prototype M600

	C-5A Aircraft (Loyd model)	**M600 prototype (Makani)**
Wing area (m^2)- A	576	35
Kite Weight (kg)	232 693	1 050
Kite coefficient of lift (C_L)	1	2
Kite coefficient of drag (C_D)	0.05	0.05
Tether coefficient of drag (C_{DT})	0.04	0.04
Lift-to-Drag ratio (L/D)	20	40
Tether's length (m)- R	400	440
Tether's working Stress (MPa)- σ	345	2 137
Tether's Density (kg/m^3)- ρ_T	8 000	1 760
Tether's Material	Steel	Carbon fibre

Looking at previous table, it's possible to see that C-5A is approximately 16 times bigger and 220 times heavier than M600, however with half of the lift coefficient. Typically, a lift coefficient of 2 is difficult to achieve, so this could be a little over estimated, but due to the Makani confidentiality, its actual value isn't really known. This discrepancy intends to show a better climbing performance by the M600 design, revealed in a higher gliding number (L/D), once the kite's drag coefficient was considered the same. The tether drag coefficient was also considered the same of C-5A because the resemblance of cylindrical shape facing the wind. However, as said before, the tether material of both devices will influence the flying performance, therefore M600's carbon fibre tether is stronger (can withstand greater tensions) and less dense than C-5A's steel tether. The drag coefficients of both the kite and tether might be improved, thanks to the surface treatment that force the turbulent boundary layer and reduce drag (similar to the effect of a golf ball surface). However, due to the uncertainty of their actual values, which still may be in research processes, they were kept the same.

4.3 Results Discussion

After setting the new inputs in Table 4.1, is possible now to re-run the model created in Chapter 3. The obtained results are presented next:

Table 4.2 Comparation between the results obtained for the C-5A and M600

	C-5A Aircraft (Loyd model)	M600 prototype (Makani)
Average power output (MW)	6.674	0.5981
Peak tether tension (MN)	2.390	0.486
Kite speed (m/s)	89.700	98.670
Average apparent speed (m/s)	90.180	99.200
Tether's thickness (cm)	9.39	4.08

Looking at Table 4.2 it's possible to verify that M600's average power output gets close to its nominal power of 600 kW. That fact reveals some consistence in the model proposed by Loyd, showing that it's possible to produce energy by the drag force actuating in a crosswind kite, which he called drag power production. Despite both kites fly at 5.5 RPM, the M600 reaches a higher apparent velocity of about 357 km/h due to its larger tether. This apparent velocity is the one which really contributes to make the turbines in the wing spinning and produce energy.

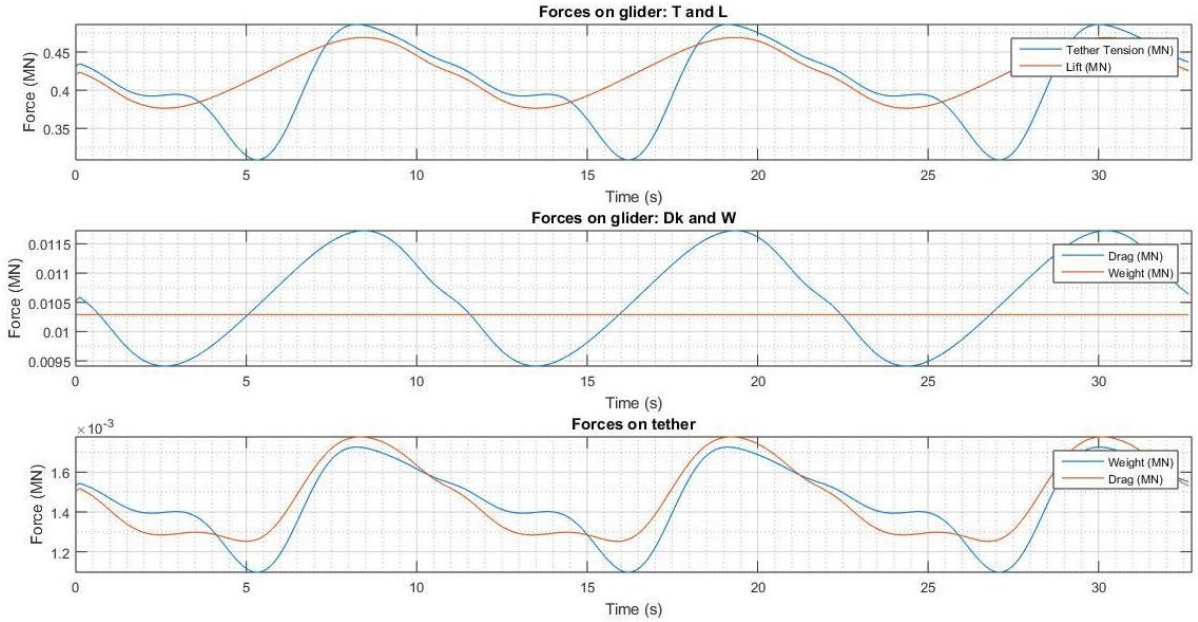

Figure 4.3 Absolute value of forces acting on M600 and his tether for three cycles of rotation

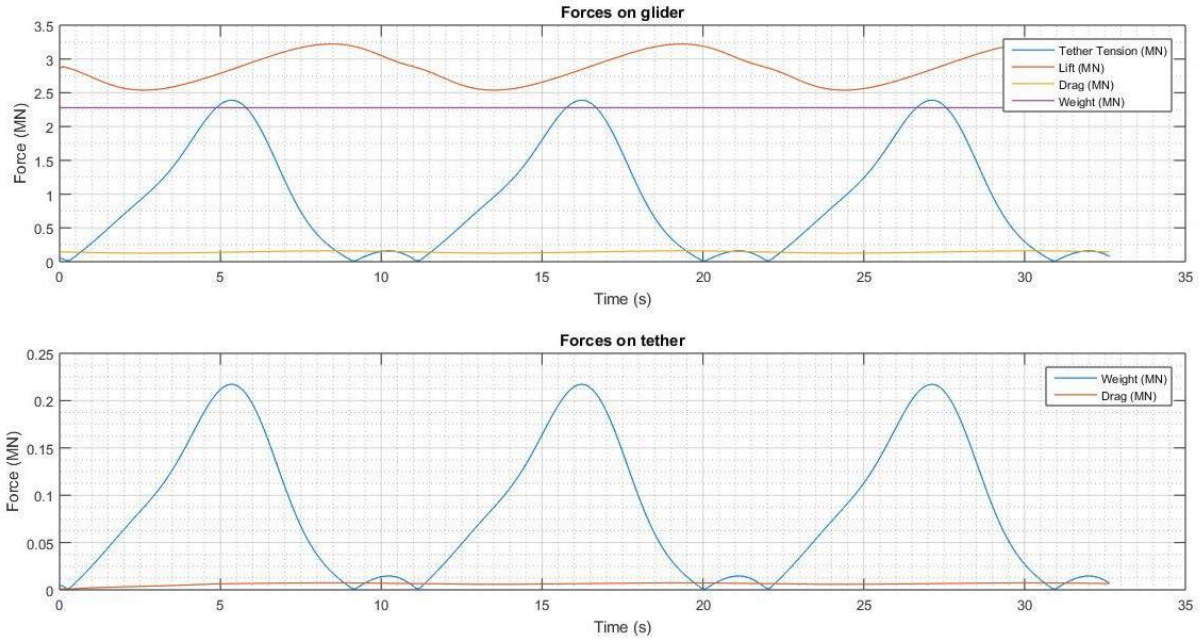

Figure 4.4 Absolute value of forces acting on C-5A and his tether for three cycles of rotation

In these two figures it's possible to see the absolute values of the forces acting in M600 (Figure 4.3) and C-5A (Figure 4.4), where the force with greater magnitude is lift, keeping the devices in the air, despite the tether tension overcome it in some instants in the case of M600. The pultruded carbon fibre material used in M600 structure grants him a low weight that can be almost negligible in the global system of forces, when compared with the C-5A weight which has more impact, like is showed in the first plot of Figure 4.4. The C-5A higher weight (either kite and tether) increases the load on the kite, meaning that it needs to generate more lift to sustain the tether with a value of around 3 MN and the opposite in the M600 kite with around 0.43 MN of magnitude. The higher density of the steel concedes to the C-5A tether a weight of about 85 kN, a higher value when compared with the carbon fibre's M600 tether with a weight of 1.4 kN approximately.

The M600 kite's drag is also minimal as in C-5A, due to their aerodynamic wings design, not affecting too much their motion. The maximum tension registered in the M600 tether was 0.49 MN, which combined with a greater carbon fibre's working stress, allows a diameter of 4 centimetres, 5 centimetres thinner tether than the C-5A one (Table 4.2). This thinner tether results in a minimal tether drag with a mean value of 1.4 kN while the C-5A tether drag has a mean value of 63 kN. However, it's important to understand if the kite can withstand the tensions induced by the tether.

The tether is capable of withstand the proposed stresses if the peak tether tension is lower than the maximum breaking tension. The maximum breaking tension is the maximum force that can be supported by the tether over its sectional area. Therefore, this value can be obtained by the product of the tether's working stress (Table 4.1) and its section area given by $\pi(d/2)^2$ (Table 4.2), due to its circular shape. That gives a maximum breaking tension of around 2.69 MN, which is a much bigger value when compared with the peak tether tension registered: 0.49 MN (Table 4.2), then this tether can withstand the proposed stresses.

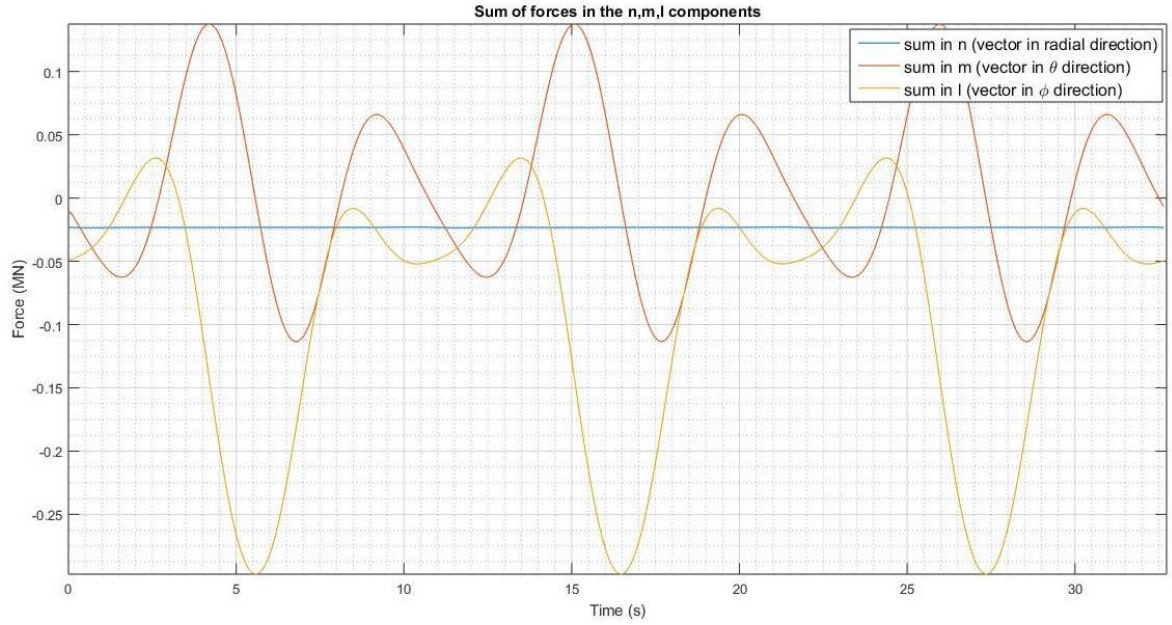

Figure 4.5 Sum of the forces actuating in the kite (lift, drag, tether tension and weight) in each components of the unit vectors l (ϕ direction), m (θ direction) and n (radial direction)

The previous figure represents the sum of the forces that act in the kite in each of their components: $\vec{l}, \vec{m}$ and $\vec{n}$. Is interesting to verify that the sum of forces acting in the kite's centre of pressure in the radial direction ($\vec{n}$) are almost null, which prove that the tether is fully extended.

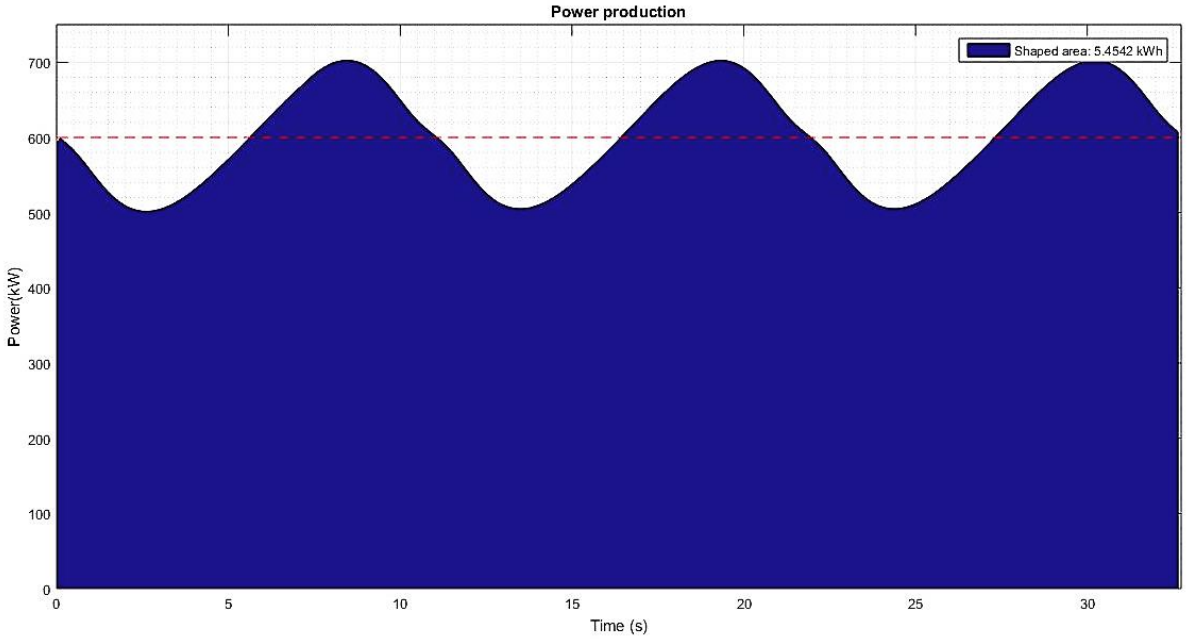

Figure 4.6 Power produced over time and respective amount of energy

The previous figure represents the variation of the power produced over time, calculated by the product between the drag power (D_P) and the apparent velocity (equation 2.23). This power drag is 1/3 of the drag which is induced in the total system, increasing them in 50%. In this plot was interesting to calculate the integral between the interval [0, 32.73] seconds, by the trapezoidal method. That gives the area of the region bounded by its graph, which corresponds to the energy produced by the M600 in three cycles of rotation, which is approximately 5.45 kWh. With the device working for one hour without any interruption, it would produce 599.92 kWh.

Still looking at this plot is possible to conclude that the turbine generators may need to be over dimensioned, to accept up to the nominal power of 600 kW, because otherwise they would be wasting energy. Typically, this phenomenon could be controlled with additional drag provoked by flaps in the wings or by the turbine rotors themselves, that lead to the reduction of the average power over cycle. This additional drag must be assured by the on-board controllers.

Chapter 5. Conclusions

In 1980, the engineer Miles L. Loyd suggested that lifting a wind turbine into the atmosphere, at some significant distance above the ground, where winds tend to blow more consistently and at greater speed than they do at ground level, could increase the energy production significantly. His suggestion was ignored for many years but in the second decade of the twenty-first century has received considerably more attention. Loyd's tested his model in a large military aircraft (C-5A), a study absolutely theoretical that intended only to demonstrate the potential that is possible to achieve from wind extraction at high altitudes (higher that 200 meters) but unfeasible in practical terms due to its high weight. In 2016, Makani company started developing the M600, a technology designed for large generating capacity that intends to accomplish Loyd's ideas for drag power production. This prototype is a substantially smaller aircraft made with different materials and autonomous controls that increase the aerodynamics of the kite.

In this dissertation, the goal was to predict the behaviour of the M600, and study how much energy he could produce. The kite takes approximately 10.91 seconds to make each full rotation in the counter-clockwise direction, with an orbit size of 0.4 radians, a constant velocity of approximately 98.67 m/s (5.5 RPM) and an average apparent velocity of 99.20 m/s which contributes to make the on-board turbines to spin and produce energy. It was considered a wind model to predict his variation with altitude, oscillating between 8.66 and 10.86 m/s to altitudes between 75 and 363 meters (Figure 3.6), however with a wind speed constant of 10 m/s the obtained results are very similar like it's showed in Table 3.3.

To maintain an accurate orbit, the flight was controlled by the variation of the tangent of the roll angle, which is defined in equation 3.6 by C letter. To re-run the Simulink model with the values of M600, it was necessary to calculate again the roll angle in equation 3.5, so the newly obtained values for *Roll angle ($\beta=0$)* and *Roll angle ($\beta=\pi$)* were -7.25 and 46.68 respectively. These values are very similar to the ones obtained for C-5A (see Attachment 3), therefore these changes in C calculation has no significant influence in the final results. It can be concluded that this control action isn't the most correct way to ensure that the kite takes the desired path. In fact, a more accurate controller should be needed that can adjust the kite in its six degrees of freedom, capable of respond within compatible time lags to disturbances in the system.

The obtained results show some consistency with the expected ones, with an average power output of 0.5981 MW, very close to the M600 nominal power and peak tether tension of 0.49 MN, a value that the kite is able to withstand. However, the turbine generators may need to be over dimensioned because the device registers values above the nominal power and in that case would be wasting energy. To assure values below the 600 kW, additional drag may be induced by flaps or by the turbine rotors.

Many assessment issues regarding safety and aviation authority, that are beyond the goal of this dissertation, must be approved before these devices can be marketed. It is important to understand the interaction of these devices within a farm, the consequences of a tether or device failure to avoid unnecessary accidents, the localization where these devices will operate that will depend on weather groundings and the ground area occupied to build a wind farm [44]. Despite this, in 2017 Makani published a 37 minutes video on their personal page at *Youtube*, showing a full test flight of the M600 prototype [45], an enticing video that shows that this prototype truly works.

5.1 Future Work

One of the challenges in this MSc dissertation was to predict the velocity of rotation, for the kite to follow the desired trajectory. So, the flight path was approached by the time function of the angular position of a uniform circular motion (equation 3.1). This approach does not portray the real behaviour of the system, since the speed of the M600 will depend on external conditions such as wind speed and although the variation of wind speed has been taken into account in the model, this revealed not to cause great changes in the output power of the system. It would be interesting to trace a power curve and calculate the capacity factor of the device with a more realistic value for the tether's coefficient of drag, using a more detailed model.

To try to solve this problem, a closed loop model was made, therefore after the calculation of $\ddot{\theta}$ and $\ddot{\emptyset}$, their integral was obtained which gives the velocity components and their second integral gives the position components: θ and $\emptyset$. In this model it wasn't necessary to resort to Rodrigues's formula or define the beta (β) parameter, since the position and velocity of rotation of the kite were calculated automatically by the model, however for the kite to follow the desired trajectory, a correct controller must be used. For that, a proportional–integral–derivative (PID) controller was tested, which is a control loop feedback mechanism. The PID controller continuously calculates an error value as the difference between a desired setpoint and a measured process variable and applies a correction based on proportional, integral, and derivative terms (denoted P, I, and D respectively). To apply this PID controller, those three terms must be defined, however after several tests the desired flight path wasn't taken, as can be seen in the Figure 5.1, with the kite describing a very irregular trajectory, which even crosses the ground with negative heights.

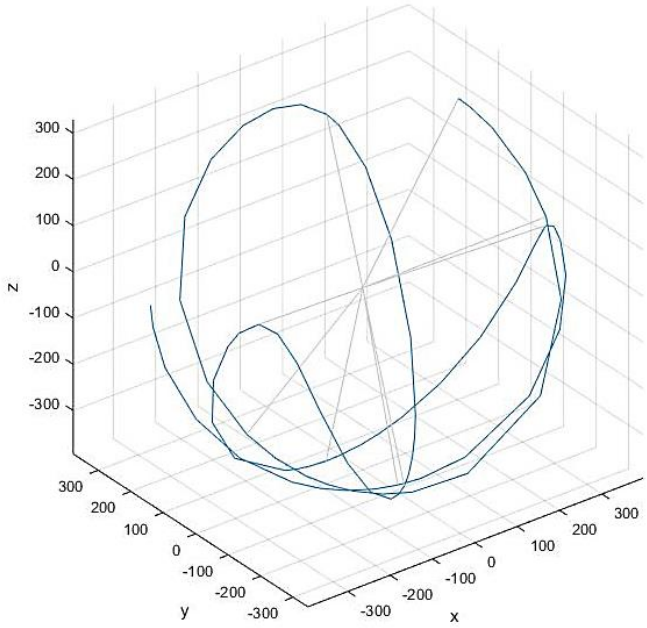

Figure 5.1 Flight path described by the kite in the closed loop model

As the results of this model did not allow to get conclusions, the open model was used in this dissertation. However, it remains open for a future study, the development of a controller that allows to rectify not

only the roll angle but also the other degrees of freedom of the kite as the yaw and pitch angles, the variation of the wind angle of attack in function of his direction and the match of kite's velocity with a realist tether drag coefficient. This implementation would improve the results of the closed loop.

It's also important to be made a future study from an economic point of view, to predict if this technology can compete with the traditional ones. The value of its operational expenditures ($OpEx_t$) is a major question which need to be clarified and will help to realize if this technology is viable. One advantage of the M600 is the use of a fixed tether length. As it isn't being always winded up and unwinded this can reduce the tether fatigue and consequently it can last longer.

The carbon fibre is much more expensive per kilogram (in the order of 90-100€/kg) than steel or fibre glass (in the order of 2-5€/kg) [46] which are the typical materials used in the construction of wind turbines. However, when comparing these two kind of technologies to harness wind energy, it's necessary to consider that they have a proportion of 1 to 260 tonnes but also have different nominal powers of 0.6 and 2 MW [47]. All these factors need to be taken into account when looking to the capital cost (CapEx) which allied with the $OpEx_t$ gives the total cost of the technology over its lifetime. The division of this cost by the value of all energy produced over its lifetime gives the levelized cost of energy (equation 1.2), that as it was previously mentioned, is one important parameter to predict if it's worth investing in this technology.

Nowadays, onshore wind power LCOE's could round the 0.05/kWh [48], and Makani claim that his prototype can reach a competitive value of 0.026 €/kWh [49], however to be able to prove this value it's necessary to continue the development of the technology towards commercial projects.

References

[1] G. M. Masters, *Renewable and Efficient Electric Power Systems*. 2004.

[2] C. L. Archer and M. Z. Jacobson, "Evaluation of global wind power," *J. Geophys. Res.*, vol. 110, no. D12, p. D12110, 2005.

[3] M. Ahmed *et al.*, "High Altitude Wind Power Systems : A Survey on Flexible Power Kites To cite this version : High Altitude Wind Power Systems : A Survey on Flexible Power Kites," pp. 2085–2091, 2012.

[4] P. Williams, B. Lansdorp, and W. Ockesl, "Optimal Crosswind Towing and Power Generation with Tethered Kites," *J. Guid. Control. Dyn.*, vol. 31, no. 1, pp. 81–93, 2008.

[5] XCompany, "Makani." [Online]. Available: https://x.company/. [Accessed: 15-Feb-2017].

[6] M. L. Loyd, "Crosswind Kite Power," *Energy*, vol. 4, no. 3, pp. 106–111, 1979.

[7] D. E. Newton, "Chapter 2. Problems, Controversies, and Solutions," in *Wind Energy: a reference handbook*, 2015, pp. 61–131.

[8] A. Cherubini, A. Papini, R. Vertechy, and M. Fontana, "Airborne Wind Energy Systems: A review of the technologies," *Renew. Sustain. Energy Rev.*, vol. 51, pp. 1461–1476, 2015.

[9] M. Diehl, "Airborne wind energy: Basic concepts and physical foundations," *Green Energy Technol.*, pp. 3–22, 2013.

[10] Stekgr (KiteGenResearch), "KiteGen STEM," 2009. [Online]. Available: http://www.kitegen.com/en/. [Accessed: 02-Feb-2017].

[11] Ampyx Power, "Technology." [Online]. Available: https://www.ampyxpower.com/. [Accessed: 04-Feb-2017].

[12] Omnidea, "Lemap." [Online]. Available: http://www.lemap.omnidea.net/. [Accessed: 05-Feb-2017].

[13] KitePower, "Technology." [Online]. Available: http://www.kitepower.eu/home/1-about.html. [Accessed: 07-Feb-2017].

[14] R. Schmehl, "Experimental setup for automatic launching and landing of a 25m2 traction kite," 2014. [Online]. Available: https://www.youtube.com/watch?v=w4oWs_zNpr8. [Accessed: 07-Feb-2017].

[15] K. Geebelen *et al.*, "An experimental test setup for advanced estimation and control of an airborne wind energy system," in *Airborne Wind Energy*, U. Ahrens, M. Diehl, and R. Schmehl, Eds. Springer, Berlin, Heidelberg, 2013, pp. 459–471.

[16] M. I. (KiteGen Research), "KiteGen Carousel," 2009. [Online]. Available: http://www.kitegen.com/en. [Accessed: 02-Feb-2017].

[17] M. Canale, L. Fagiano, and M. Milanese, "KiteGen: a revolution in wind energy," *Energy*, vol. 34, no. 3, pp. 355–361, 2009.

[18] NtsX-Wind, "nts X-Wind - So funktionert unsere Technologie," 2013. [Online]. Available: https://www.youtube.com/watch?v=8S0G23rHlo4. [Accessed: 10-Feb-2017].

[19] U. Ahrens, B. Pieper, and C. Töpfer, "Combining Kites and Rail Technology into a Traction-Based Airborne Wind Energy Plant," in *Airborne Wind Energy*, U. Ahrens, M. Diehl, and R. Schmehl, Eds. Springer, Berlin, Heidelberg, 2013, pp. 437–441.

[20] SkyWindPower, "Sky WindPower Inc. Executive Summary," 2013. [Online]. Available: http://www.skywindpower.com/. [Accessed: 12-Feb-2017].

[21] B. W. Roberts *et al.*, "Harnessing High-Altitude Wind Power," *IEEE Trans. Energy Convers.*, vol. 22, no. 1, pp. 136–144, 2007.

[22] P. Koch, H. Wernli, and H. C. Davies, "An event-based jet-stream climatology and typology," *Int. J. Climatol.*, vol. 26, no. 3, pp. 283–301, 2006.

[23] Altaeros, "Technology." [Online]. Available: http://www.altaeros.com/. [Accessed: 12-Feb-2017].

[24] J. Energy, "High-Altitude Wind Research & Development," 2008.

[25] JobyEnergyInc, "Joby Energy Airborne Wind Turbine Concept," 2010. [Online]. Available: https://www.youtube.com/watch?v=8BnKzCtGVxs. [Accessed: 13-Feb-2017].

[26] MakaniPower, "Technology." [Online]. Available: https://x.company/makani/. [Accessed: 15-Feb-2017].

[27] M. MAKINO, "(12) Patent Application Publication (10) Pub . No .: US 2006 / 0222585 A1 Figure 1," vol. 002, no. 15, p. 7, 2017.

[28] NASA, "Relative Velocities (Ground Reference)." [Online]. Available: https://www.grc.nasa.gov/www/k-12/airplane/move.html. [Accessed: 15-Sep-2017].

[29] "Forces Acting on an Airplane." [Online]. Available: http://www.pilotsweb.com/principle/forces.htm. [Accessed: 05-Jan-2018].

[30] "C-5M Super Galaxy Fact Sheets," 2006. [Online]. Available: http://www.theaviationzone.com/factsheets/c5_specs.asp. [Accessed: 10-Jan-2018].

[31] "C-5A Galaxy Gallery," 2013. [Online]. Available: https://amcmuseum.org/at-the-museum/aircraft/c-5a-galaxy/. [Accessed: 27-Mar-2018].

[32] "Simulink." [Online]. Available: https://www.mathworks.com/products/simulink.html. [Accessed: 07-Feb-2018].

[33] E. Piña, "Rotations with Rodrigues' vector," *Eur. J. Phys.*, vol. 32, no. 5, pp. 1171–1178, 2011.

[34] "Spherical coordinate system," *Coordinate system conversions*. [Online]. Available: https://en.wikipedia.org/wiki/Spherical_coordinate_system. [Accessed: 09-Nov-2017].

[35] J. R. Garratt, "Review: the atmospheric boundary layer," *Earth-Science Rev.*, vol. 37, no. 1–2, pp. 89–134, 1994.

[36] F. M. da Silva, "Theoretical classes of aerodynamics: 'A Camada Limite Atmosférica.'" Faculdade De Ciências da Universidade de Lisboa, 2016.

[37] E. W. Peterson and J. P. Hennessey, "On the Use of Power Laws for Estimates of Wind Power Potential," *Journal of Applied Meteorology*, vol. 17, no. 3. pp. 390–394, 1978.

[38] NASA, "Aircraft Roll Motion." [Online]. Available: https://www.grc.nasa.gov/www/k-12/airplane/roll.html. [Accessed: 02-Feb-2018].

[39] MISB, "MISB ST 0601.8 UAS Datalink Local Set," no. October, 2014.

[40] F. Felker, "Progress and Challenges in Airborne Wind Energy," *Airborne Wind Energy Conf. 2017*, pp. 1–4, 2017.

[41] M. Tavakkolizadeh and H. Saadatmanesh, "Strengthening of Steel-Concrete Composite Girders Using Carbon Fiber Reinforced Polymers Sheets," *J. Struct. Enginnering*, vol. 129, no. 1, pp. 30–40, 2003.

[42] Makani Power, "Response to the Federal Aviation Authority," *Docket No.: FAA-2011-1279; Notice No. 11-07 Notification for Airborne Wind Energy Systems (AWES)*, 2012. [Online]. Available: http://www.energykitesystems.net/FAA/FAAfromMakani.pdf. [Accessed: 03-Feb-2018].

[43] E. Lunney, M. Ban, N. Duic, and A. Foley, "A state-of-the-art review and feasibility analysis of high altitude wind power in Northern Ireland," *Renew. Sustain. Energy Rev.*, vol. 68, pp. 899–911, 2017.

[44] M. Barnard, "Airborne Wind Energy: It's All Platypuses Instead Of Cheetahs," 2014. [Online]. Available: https://cleantechnica.com/2014/03/03/airborne-wind-energy-platypuses-instead-cheetahs/. [Accessed: 20-Apr-2018].

[45] Makani, "Testing Makani's M600 energy kite in Spring 2017," 2017. [Online]. Available: https://www.youtube.com/watch?v=CKFlMDUHtLg&t=400s. [Accessed: 16-Feb-2018].

[46] D. R. Tobergte and S. Curtis, "Materials cost," *J. Chem. Inf. Model.*, vol. 53, no. 9, pp. 1689–1699, 2013.

[47] Piotr, "Horizontal Axis Wind Turbine – 2MW," 2009. [Online]. Available: http://etcgreen.com/horizontal-axis-wind-turbine-2mw/. [Accessed: 22-Jun-2018].

[48] IRENA, "Power Generation Costs in 2017," p. 16, 2017.

[49] M. Power, "AIRBORNE Wind Turbine (AWT)." [Online]. Available: http://www.arpae-summit.com/paperclip/exhibitor_docs/13AE/Makani_Power_5.pdf. [Accessed: 05-Jun-2018].

Attachments

Attachment 1 Input constants inserted in Matlab to build the Simulink model based on C-5A aircraft

```
% Constants LOYD VALUES
hmed=1;
hr=0.4;
R=400; %tether length (m)
Diametro=0.11;%tether diameter
A=576; %wing reference area of kite
g=9.8; % gravity acceleration (m/s2)
densi_ar=1.225; %air density (kg/m3)
densi_cable=8000; %cable density (kg/m3)
Cl=1; %coefficient of lift
Cd=0.05; %coefficient of drag
Cdt= 0.04;%coefficient of drag in tether
L_D=20; %lift-to-drag ratio
Vw=10; %Vw reference
Zref=204;%reference height to Vw=10
ws=345*10^6; %working stress (Pa)
m= 232693; %aircraft mass (kg)
W=m*g; % glider weight (N)
alpha=1/7; %alpha parameter
```

Attachment 2 Representation of the Simulink model

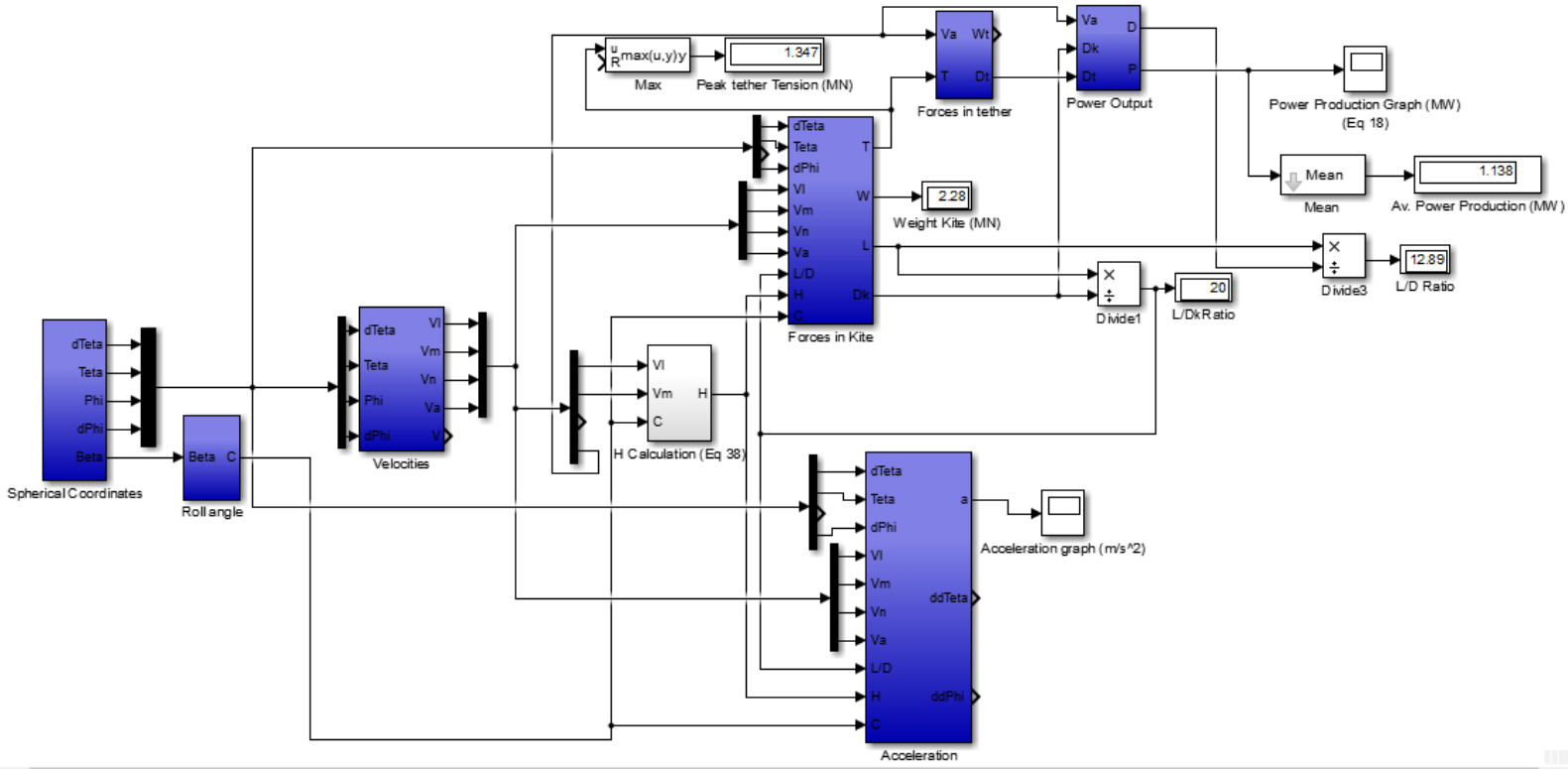

Attachment 3 Matlab 3D graph, where is represented the flight path of the C-5A aircraft at 5.5 RPM, as the vectors velocity and his absolute value, the position, and the roll angle in four positions

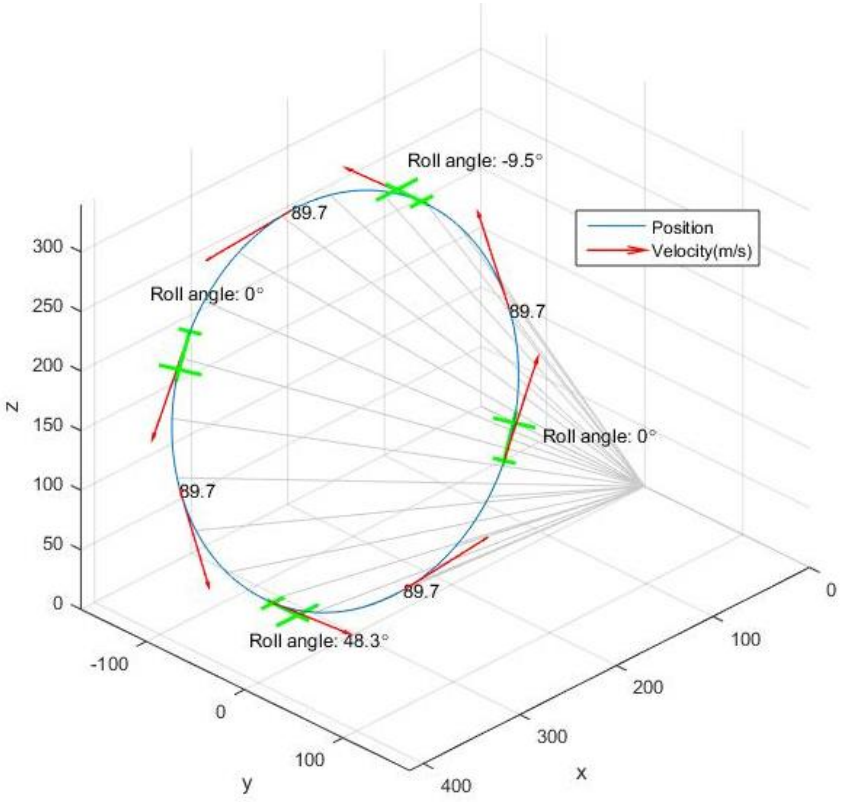

Attachment 4 Matlab graph that show the apparent and absolute velocities of the C-5A to 5.5 RPM in three cycles of rotation